



HAL
open science

Single-cell transcriptomics uncovers an instructive T-cell receptor role in adult $\gamma\delta$ T-cell lineage commitment

Sara Scaramuzzino, Delphine Potier, Robin Ordioni, Pierre Grenot,
Dominique Payet-bornet, Hervé Luche, Bernard Malissen

► **To cite this version:**

Sara Scaramuzzino, Delphine Potier, Robin Ordioni, Pierre Grenot, Dominique Payet-bornet, et al.. Single-cell transcriptomics uncovers an instructive T-cell receptor role in adult $\gamma\delta$ T-cell lineage commitment. EMBO Journal, 2022, 41, 10.15252/emj.2021110023 . hal-03763565

HAL Id: hal-03763565

<https://amu.hal.science/hal-03763565>

Submitted on 29 Aug 2022

HAL is a multi-disciplinary open access archive for the deposit and dissemination of scientific research documents, whether they are published or not. The documents may come from teaching and research institutions in France or abroad, or from public or private research centers.

L'archive ouverte pluridisciplinaire **HAL**, est destinée au dépôt et à la diffusion de documents scientifiques de niveau recherche, publiés ou non, émanant des établissements d'enseignement et de recherche français ou étrangers, des laboratoires publics ou privés.



Distributed under a Creative Commons Attribution 4.0 International License

Single-cell transcriptomics uncovers an instructive T-cell receptor role in adult $\gamma\delta$ T-cell lineage commitment

Sara Scaramuzzino^{1,2,†} , Delphine Potier^{2,†} , Robin Ordioni¹, Pierre Grenot¹,
Dominique Payet-Bornet^{2,*} , Hervé Luche^{1,**}  & Bernard Malissen^{1,2,***} 

Abstract

After entering the adult thymus, bipotent T-cell progenitors give rise to $\alpha\beta$ or $\gamma\delta$ T cells. To determine whether the $\gamma\delta$ T-cell receptor (TCR) has an instructive role in $\gamma\delta$ T-cell lineage commitment or only “confirms” a pre-established $\gamma\delta$ T-cell lineage state, we exploited mice lacking expression of LAT, an adaptor required for $\gamma\delta$ TCR signaling. Although these mice showed a T-cell development block at the CD4[−]CD8[−] double-negative third (DN3) stage, 0.3% of their DN3 cells expressed intermediate levels of $\gamma\delta$ TCR (further referred to as $\gamma\delta^{\text{int}}$) at their surface. Single-cell transcriptomics of LAT-deficient DN3 $\gamma\delta^{\text{int}}$ cells demonstrated no sign of commitment to the $\gamma\delta$ T-cell lineage, apart from $\gamma\delta$ TCR expression. Although the lack of LAT is thought to tightly block DN3 cell development, we unexpectedly found that 25% of LAT-deficient DN3 $\gamma\delta^{\text{int}}$ cells were actively proliferating and progressed up to the DN4 stage. However, even those cells failed to turn on the transcriptional program associated with the $\gamma\delta$ T-cell lineage. Therefore, the $\gamma\delta$ TCR-LAT signaling axis builds upon a $\gamma\delta$ T-cell uncommitted lineage state to fully instruct adult $\gamma\delta$ T-cell lineage specification.

Keywords T cell; development; $\gamma\delta$ T-cell lineage specification; single-cell transcriptomics

Subject Categories Immunology; Signal Transduction

DOI 10.15252/emboj.2021110023 | Received 24 October 2021 | Revised 18 December 2021 | Accepted 3 January 2022 | Published online 7 February 2022

The EMBO Journal (2022) 41: e110023

Introduction

In mice, most T cells express a T-cell antigen receptor (TCR) consisting of α and β chains, whereas a smaller population expresses an alternative form made of γ and δ chains. The TCR α , β ,

γ , and δ chains each contains a clonally variable (V) region that participates to antigen recognition. During intrathymic T-cell development, the genes coding for TCR V regions assemble via site-specific DNA recombinations that can result in productive, or in out-of-frame non-productive rearrangements. Upon thymus colonization, T-cell precursors develop into CD4[−]CD8[−] double-negative (DN) cells. Based on the expression of CD25 and CD44, DN cells can be organized according to the following developmental series: DN1 (CD44⁺CD25[−]) → DN2 (CD44⁺CD25⁺) → DN3 (CD44[−]CD25⁺) → DN4 (CD44[−]CD25[−]). DN3 cells simultaneously rearrange the *Trb*, *Trg*, and *Trd* genes that code for the TCR β , γ , and δ chains, respectively (Livak *et al*, 1999). Upon productive rearrangement of *Trg* and *Trd* genes, DN3 cells express a $\gamma\delta$ TCR and in turn mature into CD4[−]CD8[−] $\gamma\delta$ T cells. Unlike conventional $\alpha\beta$ T cells that acquire their effector function in the periphery, a large fraction of $\gamma\delta$ T cells commit to an effector fate during intrathymic development. After migrating to the periphery and predominantly colonizing epithelial barriers, these “innate-like” $\gamma\delta$ T cells had the capacity to respond without delay to infection and tissue damage (Prinz *et al*, 2013; Hayday, 2019; Contreras & Wiest, 2020; Fiala *et al*, 2020; Parker & Ciofani, 2020; Hosokawa & Rothenberg, 2021). Upon productive *Trb* gene rearrangements, DN3 cells produce TCR β chains that associate with invariant pre-TCR alpha (pT α) chains to give rise to a pre-TCR (Dutta *et al*, 2021). Pre-TCR⁺ DN3 cells develop into CD4⁺CD8⁺ double-positive (DP) cells that rearrange *Tra* genes that code for TCR α chains. On productive *Tra* gene rearrangements and replacement of pT α by TCR α , the resulting TCR $\alpha\beta$ ⁺ DP cells undergo positive and negative selection to generate CD4⁺ and CD8⁺ single-positive (SP) cells that leave the thymus. $\gamma\delta$ T-cell development is thus punctuated by a single checkpoint termed $\gamma\delta$ selection and operated by the $\gamma\delta$ TCR, whereas $\alpha\beta$ T-cell development is subjected to two sequential checkpoints termed β and $\alpha\beta$ selection and operated by the pre-TCR and $\alpha\beta$ TCR, respectively. Those checkpoints are intended to couple T-cell development to the prior achievement of productive

¹ Centre d'Immunophénomique (CIPHE), Aix Marseille Université, INSERM, CNRS UMR, Marseille, France

² Centre d'Immunologie de Marseille-Luminy (CIML), Aix Marseille Université, INSERM, CNRS, Marseille, France

*Corresponding author: Tel: +33 491269143; E-mail: payet@ciml.univ-mrs.fr

**Corresponding author: Tel: +33 675916762; E-mail: herve.luche@inserm.fr

***Corresponding author: Tel: +33 491269402; E-mail: bernardm@ciml.univ-mrs.fr

[†]These authors contributed equally to this work

TCR gene rearrangements and the ensuing expression of $\alpha\beta$ and $\gamma\delta$ TCR. Developing T cells that fail crossing them are thus eliminated.

The pre-TCR, $\alpha\beta$ TCR, and $\gamma\delta$ TCR associate with CD3 subunits that contain tyrosine-based activation motifs. Upon phosphorylation by the LCK protein tyrosine kinase (PTK), these motifs recruit the PTK ZAP-70 that in turn phosphorylates the adaptor protein LAT, resulting in the assembly of a LAT signalosome which mediates most of the TCR-induced transcriptional responses (Mori *et al*, 2021). The requirement for pre-TCR and $\gamma\delta$ TCR signaling during early T-cell development can be documented by the arrest of $\alpha\beta$ and $\gamma\delta$ T-cell development at the DN3 stage in mice deficient in most CD3 subunits or LAT (Malissen *et al*, 1999; Munoz-Ruiz *et al*, 2016). Two models have been proposed to explain how DN3 cells engage into the $\alpha\beta$ or $\gamma\delta$ T-cell lineage (reviewed in Parker & Ciofani, 2020). The precommitment (or stochastic selective) model postulates that $\alpha\beta$ versus $\gamma\delta$ T-cell lineage commitment is determined prior to and independently of the outcome of *Trb*, *Trg*, and *Trd* gene rearrangements. Accordingly, only those thymocytes whose predetermined lineage-specific molecular “wiring” matches the distinct signals delivered by the stochastically expressed pre-TCR or $\gamma\delta$ TCR are able to further develop. In contrast, the instructive model of $\alpha\beta$ versus $\gamma\delta$ T-cell lineage commitment posits that it is the distinct qualitative or quantitative characteristics of the pre-TCR and $\gamma\delta$ TCR signals received by DN3 cells that specify the $\alpha\beta$ versus $\gamma\delta$ lineage choice, respectively. The observation that a single transgenic $\gamma\delta$ TCR was capable of triggering $\alpha\beta$ lineage specification, upon attenuation of its signaling output (Haks *et al*, 2005; Hayes *et al*, 2005; Ciofani *et al*, 2006; Zhao *et al*, 2019), led to refine the instructive model into a signal strength model of $\alpha\beta$ versus $\gamma\delta$ T-cell lineage commitment in which the pre-TCR and $\gamma\delta$ TCR were postulated to deliver weak and strong signals, respectively. In contrast, the fate of IL17-producing ($T\gamma\delta 17$) $\gamma\delta$ T cells that arise during fetal life appears determined prior to the onset of TCR gene rearrangement, suggesting that some $\gamma\delta$ T-cell subsets might develop according to a precommitment model (Melichar *et al*, 2007; Spidale *et al*, 2018).

Mouse T-cell developmental stages are generally well distinguished by combinations of cell surface markers. However, individual T cells within a defined developmental stage might still display some heterogeneity reflecting different developmental potential, an issue that cannot be unveiled by “bulk” transcriptomic studies (Mingueneau *et al*, 2013; Roels *et al*, 2020). In contrast, single-cell RNA sequencing (scRNAseq) permits to analyze genome-wide RNA expression at single-cell levels and to determine the degree of transcriptomics heterogeneity of a given T-cell precursor population (Klein *et al*, 2019, Oh *et al*, 2021, Rothenberg, 2021, Sagar *et al*, 2020). Here, we used scRNAseq to analyze the developmental bifurcation leading to $\alpha\beta$ and $\gamma\delta$ T cells in the thymus of adult wild-type (WT) and LAT-deficient mice. It allowed us to assess whether $\gamma\delta$ TCR signals build upon a “blank slate” to initiate $\gamma\delta$ T-cell lineage specification or limit their role to “confirm” a $\gamma\delta$ T-cell transcriptional choice made prior to *Trg* and *Trd* gene rearrangements. Moreover, it provided an unprecedented single-cell resolution view of the commonalities and differences in the transcriptional signatures resulting from pre-TCR, $\gamma\delta$ TCR, and $\alpha\beta$ TCR signaling at distinct stages of adult intrathymic development.

Results

scRNAseq analysis of the developmental bifurcation leading to $\alpha\beta$ and $\gamma\delta$ T cells in adult thymus

To investigate the developmental bifurcation leading to $\alpha\beta$ and $\gamma\delta$ T-cell lineage specification at single-cell resolution, DN cell subsets encompassing such bifurcation were isolated from 6- to 8-week-old thymus using established cell surface markers, and subjected to scRNAseq (Fig 1A). Considering that DN cells represent a quantitatively minor fraction of adult thymus, 50 WT thymi were harvested, pooled, and first depleted of DP and SP cells. Using multiparameter flow cytometry, the remaining DN cells were sorted into five subsets corresponding to DN3a cells, β -selected $\alpha\beta$ precursors (DN3b TCR $\gamma\delta^-$ and DN4 TCR $\gamma\delta^-$; in short DN3b $\gamma\delta^-$ and DN4 $\gamma\delta^-$), $\gamma\delta$ -selected $\gamma\delta$ precursors (DN3b TCR $\gamma\delta^+$; in short DN3b $\gamma\delta^+$), and immature $\gamma\delta$ T cells in the process of functional diversification (DN4 TCR $\gamma\delta^+$; in short DN4 $\gamma\delta^+$) (Fig 1B and C). To facilitate subsequent merging of the five individual scRNAseq datasets, 500 splenic B cells were added as an internal standard to each sorted thymocyte subset prior to subjecting them to scRNAseq (see Materials and Methods). After quality control of sequencing data, which included the removal of low-quality cells expressing < 200 genes or expressing higher than 15% mitochondrial genes, the five scRNAseq datasets were merged into Dataset 1 (see Materials and Methods and Data Availability).

To visualize transcriptomic heterogeneity among Dataset 1 cells, we performed a non-linear dimensionality reduction using Uniform Manifold Approximation and Projection (UMAP) method. The clusters corresponding to spike-in B cells were identified in each sample based on *Cd74*, *Cd19*, and *Ms4a1* expression. Their positions fully overlapped, indicating no batch-associated variability and precluding application of corrective measure to Dataset 1. After removing clusters corresponding to non-T cells and to low-quality cells showing a reduced expression of transcripts coding for the CD3 δ and CD3 ϵ subunits of the TCR-CD3 complex, or a low percentage of ribosomal genes, the resulting Dataset 1 comprised of 57817 DN cells corresponding to 7520 DN3a, 11389 DN3b $\gamma\delta^+$, 8010 DN4 $\gamma\delta^+$, 18677 DN3b $\gamma\delta^-$, and 12221 DN4 $\gamma\delta^-$ cells.

Single-cell transcriptomics analysis of the earliest steps of $\gamma\delta$ and $\alpha\beta$ T-cell commitment

Congruent with current models of $\alpha\beta$ and $\gamma\delta$ T-cell commitment (Parker & Ciofani, 2020), the UMAP plot corresponding to Dataset 1 showed two well-separated branches emerging from DN3a cells (Fig 2A). One branch corresponded to the $\alpha\beta$ T-cell lineage and was made of DN3b $\gamma\delta^-$ and DN4 $\gamma\delta^-$ cells, whereas the other branch corresponded to the $\gamma\delta$ T-cell lineage and was made of DN3b $\gamma\delta^+$ and DN4 $\gamma\delta^+$ cells. Eleven cell clusters were identified by unsupervised analysis (Fig 2B; see Materials and Methods). DN3a cells mostly corresponded to a single cluster (cluster 2), whereas DN3b $\gamma\delta^+$ and DN4 $\gamma\delta^+$ cells comprised of two (3 and 6) and three (7, 8, and 9) clusters, respectively. DN3b $\gamma\delta^-$ and DN4 $\gamma\delta^-$ cells comprised of clusters 10, 0, and 1, and clusters 4, 5, and 11, respectively.

The $\gamma\delta$ TCR-induced DN3a \rightarrow DN3b $\gamma\delta^+$ transition is associated with a wave of cell proliferation (Prinz *et al*, 2006; Taghon *et al*,

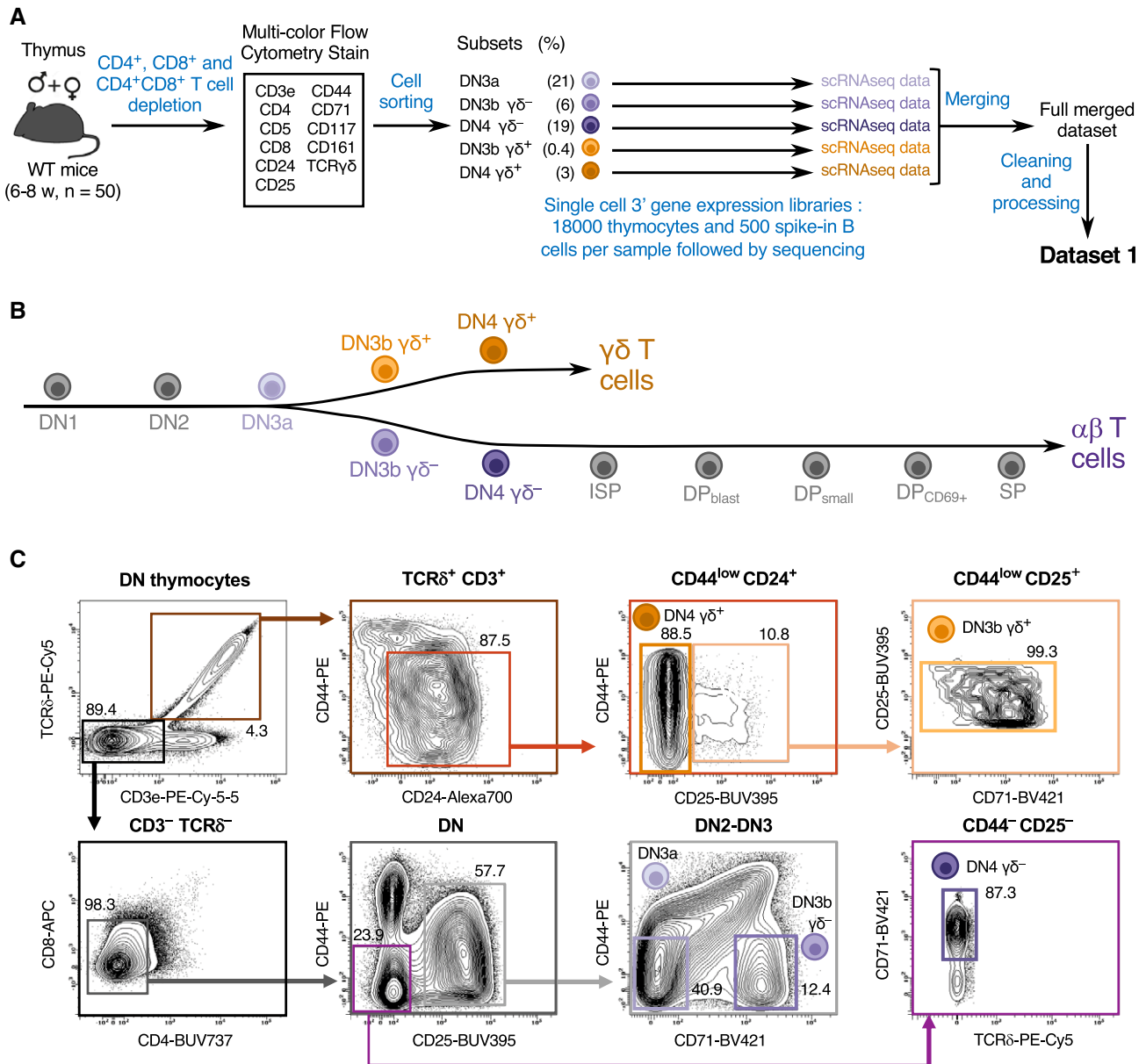


Figure 1. Schematic of scRNAseq experimental procedures.

A Schematic representation of the workflow used for scRNAseq analysis of thymus and the generation of Dataset 1. Thymi were pooled from 6- to 8-week-old C57BL/6 female ($n = 25$) and male ($n = 25$) mice. Five single-cell 3' gene expression libraries containing 18,000 thymocytes and 500 spike-in B cells were constructed and individually sequenced.

B Schematic representation of intrathymic T-cell development stages. T-cell subsets straddling the bifurcation leading to $\alpha\beta$ and $\gamma\delta$ T cells were sorted and are colored in purple or brown, respectively.

C Workflow used to sort the T-cell subsets of interest. Thymocytes were first depleted from DP and SP T cells and then sorted by FACS. The sequential gating strategy used for sorting DN3a, DN3 $\gamma\delta^+$, DN4 $\gamma\delta^+$, DN3b $\gamma\delta^-$, and DN4 $\gamma\delta^-$ subsets is shown on the specified contour plots. CD71 expression was used to distinguish post- β -selected CD44⁻CD25⁺ DN3b $\gamma\delta^-$ cells from unselected CD44⁻CD25⁺ DN3a cells. DN4 $\gamma\delta^-$ cells constitute the progeny of DN3b $\gamma\delta^-$ cells and were characterized by their CD71⁺CD44⁺CD25⁻ phenotype. The DN thymocytes gate corresponds to viable NK1.1⁻ cells. Among TCR δ^+ CD3⁺ DN thymocytes, CD24⁺CD44^{low} cells correspond to DN3b $\gamma\delta^+$ and DN4 $\gamma\delta^+$ cells. DN3b $\gamma\delta^+$ constitutes an intermediate stage bridging the DN3a and DN4 $\gamma\delta^+$ stages, whereas DN4 $\gamma\delta^+$ cells constituted the end product of the intrathymic $\gamma\delta$ developmental pathway characterized here. TCR δ^+ CD3⁺ DN thymocytes, CD24⁺CD44^{high} cells (termed "cluster B"; (Prinz *et al*, 2006)) that contain NK-like T cells. Numbers indicate percentages of cells found in each of the specified gates.

2006), and most DN3b $\gamma\delta^+$ cells were thus in the S (cluster 6) and G2/M (cluster 3) phases of the cell cycle and corresponded to transit-amplifying cells (Fig 2C). The functional diversification that occurred

in DN4 $\gamma\delta^+$ cells (see below) was associated with a return to a non-proliferative state (clusters 7, 8, and 9). As expected on the basis of former studies (Mingueneau *et al*, 2013), both DN3b $\gamma\delta^-$ and DN4

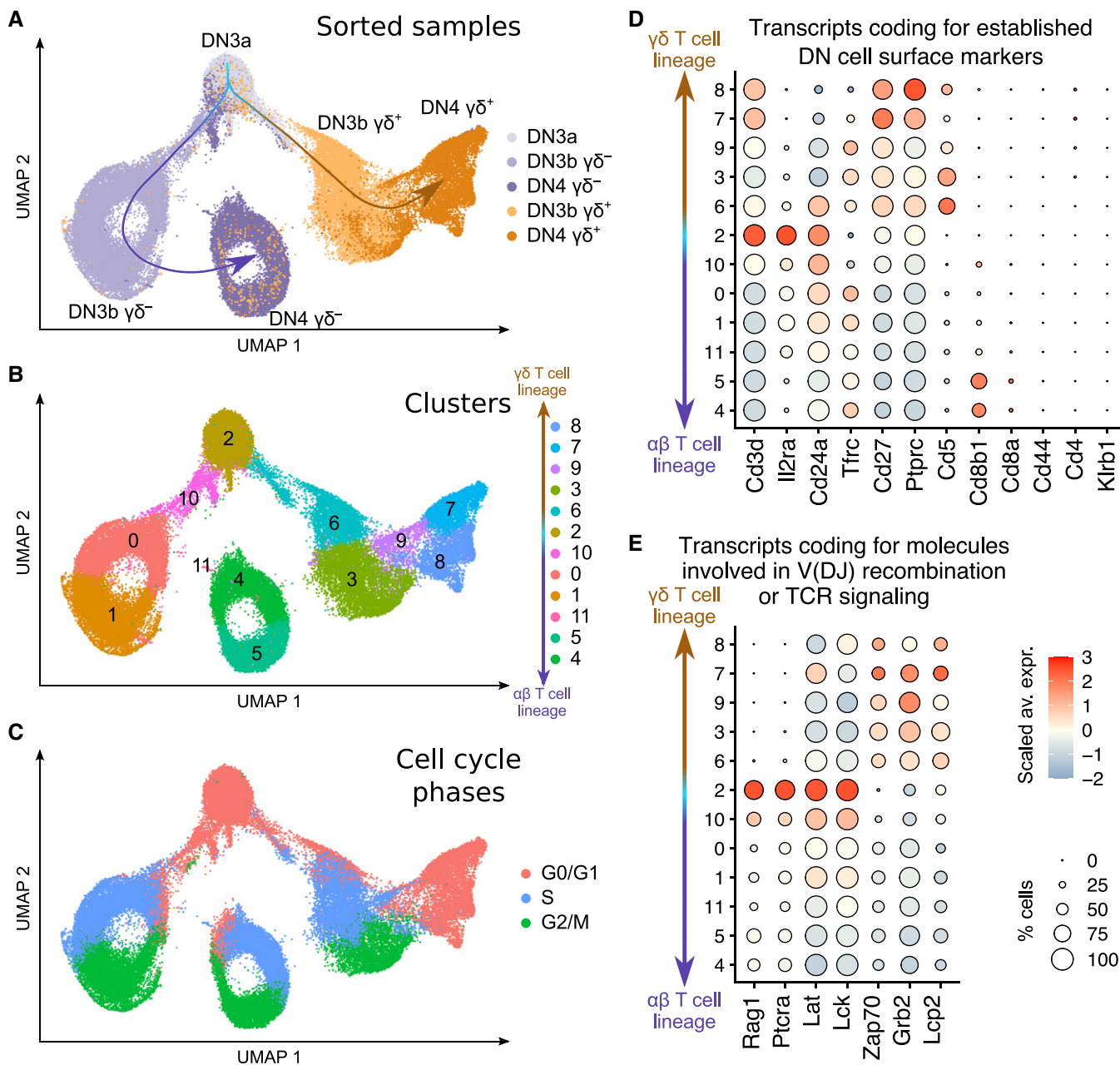


Figure 2. Single-cell RNAseq profiling of WT DN3 and DN4 adult thymocytes.

A–C UMAP plots of Dataset 1 which contains five merged scRNAseq datasets corresponding to DN3b $\gamma\delta^+$, DN4 $\gamma\delta^+$, DN3a, DN3b $\gamma\delta^-$, and DN4 $\gamma\delta^-$ sorted cells and from which the small numbers of contaminating non-T cells were excluded. Cell clustering was performed using a resolution of 0.4. The UMAP plots are colored according to the sorted cell samples (A), cell clusters (B), and cell cycle phases (C).

D, E Dot plots showing the expression level of transcripts coding for established markers of intrathymic T-cell differentiation (D), and for molecules involved in V(D)J recombination and TCR signaling (E). In (D and E), dot color represents the scaled average expression of the specified gene across the various clusters, and dot size indicates the percentage of cells expressing the specified gene.

$\gamma\delta^-$ cells constituted transit-amplifying cells. For instance, although a small fraction of DN3b $\gamma\delta^-$ cells was in G0/G1 (cluster 10), their majority was in S (cluster 0) and G2/M (cluster 1) phases. Likewise, most DN4 $\gamma\delta^-$ were in S (cluster 4) and G2/M (cluster 5) phases.

The analysis of well-characterized cell surface markers of DN cell subsets validated our sorting strategy (Fig 2D). For instance, DN3a

cells were the sole to express high levels of *Il2ra* which codes for CD25 (the interleukin 2 receptor α chain), and all the analyzed DN3–DN4 subsets were negative for *Cd44* (a DN1–DN2 cell marker) and *Klrb1* (a natural killer (NK) cell marker). *Cd8b1* that codes for the β chain of CD8 $\alpha\beta$ heterodimers started to be expressed in DN4 $\gamma\delta^-$ that are the direct precursors of immature single-positive (ISP) cells,

an intermediate CD8⁺CD4⁻ stage bridging the DN4 and CD8⁺CD4⁺ DP stages. Consistent with their robust proliferation, DN3b $\gamma\delta^+$, DN3b $\gamma\delta^-$, and DN4 $\gamma\delta^-$ cells expressed *Tfrc* transcripts that code for the transferrin receptor (also known as CD71; Kelly *et al*, 2007). As expected, expression of *Cd24* persisted in DN3b $\gamma\delta^-$ and DN4 $\gamma\delta^-$ cells and started decreasing in immature DN4 $\gamma\delta^+$ prior to their differentiation into peripheral mature CD24⁻ TCR $\gamma\delta^+$ cells (Parker & Ciofani, 2020). Finally, $\gamma\delta$ selection triggered a stronger increase in the expression of *Cd5* and *Cd27* (that codes for TNFRSF7, a member of the tumor necrosis factor receptor superfamily) as compared to β selection.

Among the analyzed DN cell subsets, DN3a cells rearrange the *Trg*, *Trd*, and *Trb* genes and decode the first pre-TCR or $\gamma\delta$ TCR signals (Klein *et al*, 2019). They expressed the highest levels of transcripts coding for the RAG1 V(D)J recombinase subunit, the pT α chain (coded by *Ptcr*), the Src family protein tyrosine kinase (PTK) LCK, and the LAT transmembrane adaptor (Fig 2E). In contrast, when compared to $\gamma\delta^-$ and β -selected cells, DN3a cells expressed the lowest levels of transcripts coding for ZAP-70, which belongs to the Syk PTK family. This finding is consistent with the expression in DN3a cells of high levels of transcripts coding for the SYK PTK, which is the eponymous member of the Syk family and can substitute for ZAP-70 (Muro *et al*, 2018). Moreover, as suggested by a former study (Palacios & Weiss, 2007), the increase in *Zap70* transcripts observed in DN3b $\gamma\delta^-$ and DN4 $\gamma\delta^-$ cells likely boosts pre-TCR signals until the ISP stage is reached. Post-selected DN3b $\gamma\delta^+$ and DN4 $\gamma\delta^+$ cells expressed the highest levels of transcripts coding for ZAP-70 and for the intracytoplasmic adaptors SLP-76 (encoded by *Lcp2*) and GRB2 among Dataset 1 cell clusters, likely contributing to reinforce the signaling strength of the $\gamma\delta$ TCR as compared to that of the pre-TCR.

Functional diversification of adult DN4 $\gamma\delta^+$ cells

A recent scRNAseq-based study compared $\gamma\delta$ T-cell functional diversification in fetal and adult thymus (Sagar *et al*, 2020). By zooming on the scRNAseq datasets corresponding to DN3a, DN3b $\gamma\delta^+$, and DN4 $\gamma\delta^+$ cells, we were able to explore further $\gamma\delta$ T-cell functional diversification in adult thymus (Fig 3A). Twelve cell clusters were identified among them using unsupervised hierarchical clustering with a fine-grained resolution. DN3b $\gamma\delta^+$ cells comprised of clusters 6, 9, 10, and 17, whereas DN4 $\gamma\delta^+$ cells comprised of clusters 11, 12, 14, 15, 18, and 22. Using differential gene expression analysis, we identified the top 6 differentially expressed genes (DEG) markers of each cluster based on the best positive log fold change, and we organized them into a dot plot (Fig 3B).

Cluster 19 was contiguous to cluster 0 (DN3a cells), and the cells it contained (a mix of DN3a and DN3b $\gamma\delta^+$ cells) started expressing *Gnl3* that codes for guanine nucleotide-binding protein-like 3 (GLN3

or nucleostemin; Fig 3B and C), suggesting their entry in the G1 phase of the cell cycle (Qu & Bishop, 2012). Consistent with our global analysis of Dataset 1 (Fig 2C), most of the remaining DN3b $\gamma\delta^+$ clusters were in S or G2/M phase (Appendix Fig S1). Following such proliferative burst, the resulting DN4 $\gamma\delta^+$ cells were predominantly resting and differentiated into IFN- γ -producing (T $\gamma\delta$ 1) and T $\gamma\delta$ 17 $\gamma\delta$ T-cell subsets. For instance, the expression of *Sox13*, a key transcription factor for T $\gamma\delta$ 17 programming (Melichar *et al*, 2007), was first induced in cluster 18 which bridged cluster 19 of DN3b $\gamma\delta^+$ cells to clusters 11 and 15 of DN4 $\gamma\delta^+$ cells (Fig 3A). Both clusters 11 and 15 expressed *Blk* and *Maf*, two T $\gamma\delta$ 17-cell hallmarks (Zuberbuehler *et al*, 2019) in addition to *Sox13* (Fig 3B and C). Cluster 15 also expressed *Rorc* which codes for the nuclear receptor ROR gamma transcription factor that governs IL-17 expression (Ivanov *et al*, 2006), whereas cluster 11 expressed *Gzma* and might correspond to a novel subset of granzyme A⁺ $\gamma\delta$ T cells endowed with cytotoxic activity (Sagar *et al*, 2020).

The T $\gamma\delta$ 1 functional branch was best characterized by the expression of high levels of *Ikzf2*, which codes for the zinc finger protein Helios, and it comprised three clusters (12, 14, and 22) (Fig 3A–C). Cluster 22 expressed *Il2rb* and *Eomes*, two hallmarks of the T $\gamma\delta$ 1 cell subset. Conversely, *Il2rb* was not expressed in cluster 14 which instead expressed the sphingosine-1-phosphate receptor (*S1pr1*) that is critical for thymocyte egress (Carlson *et al*, 2006). Cluster 14 included a subset expressing *Ccr9*, a chemokine receptor involved in migration of $\gamma\delta$ T cells to peripheral sites (Uehara *et al*, 2002). As recently suggested (Sagar *et al*, 2020), these *S1pr1*⁺ *Ccr9*⁺ cells likely correspond to a population of $\gamma\delta$ T cells that leaves the thymus in a naive state and undergoes functional polarization in the periphery. Most cells of cluster 12 corresponded to a transitional cluster between DN3b $\gamma\delta^+$ cells and the T $\gamma\delta$ 1 clusters. The remaining cells found in cluster 12 expressed *Zbtb16* (that encodes PLZF, a lineage marker of NKT cells), suggesting that they are primed toward an IFN- γ /IL4-producing fate (Kreslavsky *et al*, 2009). Therefore, our fine-grained scRNAseq analysis of DN4 $\gamma\delta^+$ cells permitted to refine a recent model of adult intrathymic $\gamma\delta^+$ T-cell functional diversification (Sagar *et al*, 2020).

Identifying the transcriptional signatures induced by the pre-TCR and $\gamma\delta$ TCR in adult thymus

To characterize early $\gamma\delta$ T-cell specification, we identified those transcripts that were differentially expressed between the DN3b $\gamma\delta^+$ and DN3b $\gamma\delta^-$ cells. Transcripts linked to cell cycling and metabolic activity were excluded from such “ $\gamma\delta$ TCR-induced signature” since most of them were induced in both the DN3b $\gamma\delta^-$ and DN3b $\gamma\delta^+$ transit-amplifying cells. Likewise, most of the transcripts typifying DN3a cells were repressed at both the DN3a \rightarrow DN3b $\gamma\delta^+$ and DN3a \rightarrow DN3b $\gamma\delta^-$ transitions (Mingueneau *et al*, 2013;

Figure 3. Intrathymic diversification of adult $\gamma\delta$ T cells.

- UMAP plots focusing on DN3a, DN3b $\gamma\delta^+$, and DN4 $\gamma\delta^+$ cells from Dataset 1. Clustering was performed using a 1.5 resolution. The UMAP plot is colored according to clusters and the main characteristics of the defined clusters specified in the right margin.
- Dot plot showing the expression level of the top 6 DEG markers characterizing each of the 12 clusters. Dot color represents the scaled average expression of the specified gene across the 12 clusters, and dot size indicates the percentage of cells expressing the specified gene.
- UMAP plots colored according to the expression level of the specified genes.

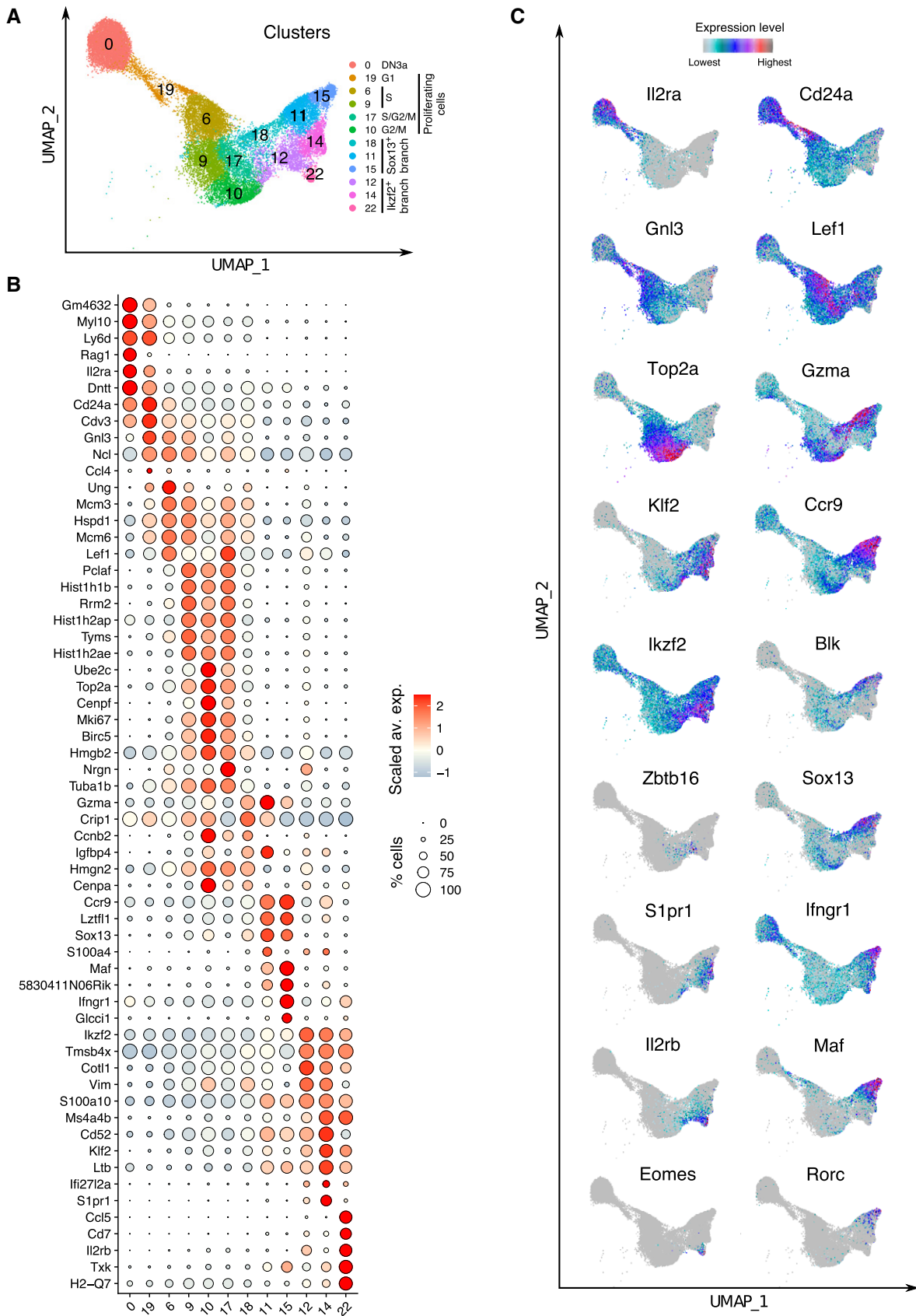


Figure 3.

Rothenberg, 2019) and thus excluded from the $\gamma\delta$ TCR-induced signature, allowing to specifically focus on transcripts associated with early $\gamma\delta$ T-cell specification. DEG with an adjusted P -value of 0 and expressed in $< 25\%$ of the DN3b $\gamma\delta^-$ cells were selected to generate the $\gamma\delta$ TCR-induced signature (Fig 4A). Using the AUCell tool (see Materials and Methods; Aibar et al, 2017), we identified which cells expressed the $\gamma\delta$ TCR-induced signature among the sorted cell subsets present in Dataset 1 (Fig 4B). As expected for a $\gamma\delta$ TCR-induced signature, DN3a cells showed the lowest AUCell scores, whereas high AUCell scores were only observed for DN3b $\gamma\delta^+$ and DN4 $\gamma\delta^+$ cells. To define a “pre-TCR-induced” signature, we took in consideration that the transit-amplifying cells of the $\alpha\beta$ T-cell lineage branch comprised both DN3b $\gamma\delta^-$ and DN4 $\gamma\delta^-$ cells (Fig 2). Therefore, for the sake of symmetry, the genes that were differentially expressed between the DN3b $\gamma\delta^-$ /DN4 $\gamma\delta^-$ cells and DN3b $\gamma\delta^+$ cells were used to define the pre-TCR-induced signature and identify genes linked to early $\alpha\beta$ T-cell specification (Fig EV1).

Commonalities and differences in the transcriptional signatures induced by the pre-TCR and $\gamma\delta$ TCR in adult thymus

The pre-TCR-induced signature was narrower than the $\gamma\delta$ TCR-induced signature and limited to 10 genes (Fig EV1). Among them, *Cd8b1* transcripts that code for CD8 β were the sole to be strongly induced during the DN3a \rightarrow DN3b $\gamma\delta^-$ /DN4 $\gamma\delta^-$ transition (Fig EV1). *Spats2* transcripts, which code for a protein involved in cell proliferation and called spermatogenesis-associated serine-rich protein (Dong et al, 2020), were also induced during this transition, although to a smaller extent than *Cd8b1* transcripts. The remaining eight genes of the pre-TCR-induced signature corresponded to genes that are expressed in DN3a cells and poorly repressed during the DN3a \rightarrow DN3b $\gamma\delta^-$ /DN4 $\gamma\delta^-$ transition as compared to the strong repression they are subject to during the DN3a \rightarrow DN3b $\gamma\delta^-$ transition. Some of them were fully repressed at the subsequent ISP stage (*Ptcra*), or reused in DP_{small} cells for *Tcra* gene rearrangements (*Rag1*) or signaling (*Dgkeos* transcripts coding for diacylglycerol kinase DGK ϵ) (Mingueneau et al, 2013). Therefore, much of the transcriptional changes induced by both the pre-TCR and $\gamma\delta$ TCR corresponded to the shutdown of the DN3a program or to the upregulation of genes involved in the cell cycle or metabolic activity. Aside from this shared component, the remaining part of pre-TCR- and $\gamma\delta$ TCR-induced transcriptional signatures markedly differed (Figs 4A and EV1). The former was primarily limited to the *Cd8b1* transcript, whereas the later consisted of a multitude of transcripts coding for proteins necessary for the functional maturation and the ensuing intrathymic differentiation of $\gamma\delta$ T cells (*Klf2*, *Pdcd1*, *Cd5*, *Cd6*, *Cd52*, *Cd53*, *Cpa3*, *Blk*, *Etv5*, and *Sox13*).

Identifying the transcriptional signatures induced by the $\alpha\beta$ TCR in adult thymus

To compare the $\gamma\delta$ TCR-induced transcriptional signature to that induced by the fully assembled $\alpha\beta$ TCR at the DP_{small} \rightarrow DP_{CD69+}/SP transition, we generated two additional scRNAseq datasets. They corresponded to adult DN and total thymocytes that were each sorted for live cells, subjected to droplet-based scRNA sequencing, and finally merged into Dataset 2 (Fig EV2A and see Materials and Methods). After controlling the quality of data merging, our clustering analysis identified nine clusters that were assigned to DN1/DN2, DN3a, DN3b/DN4, ISP/DP_{blast}, DP_{small}, DP₆₉₊, SP, and $\gamma\delta$ T cells on the basis of markers commonly used to delineate adult thymic cell subsets (Fig EV2B and C). We used Dataset 2 to define DEG between the DP_{CD69+}/SP cells and DP_{small} cells. Such “ $\alpha\beta$ TCR-induced signature” comprised of transcripts coding for transmembrane receptors important for $\alpha\beta$ T-cell function (*Cd2*, *Cd5*, *Cd69*, and *Cd53*), and for differentiation (*Tox*) and survival (*Bcl2*) (Fig EV3A), consistent with a former bulk transcriptomics study (Mingueneau et al, 2013).

Commonalities and differences in the transcriptional signatures induced by the $\gamma\delta$ TCR and $\alpha\beta$ TCR in adult thymus

When the $\gamma\delta$ TCR-induced signature was applied to Dataset 2 (Fig 4C), high AUCell scores were observed for both $\gamma\delta$ T cells and DP_{CD69+}/SP cells, suggesting that a part of the $\gamma\delta$ TCR-induced signature is also induced by the $\alpha\beta$ TCR during the DP_{small} \rightarrow DP_{CD69+}/SP transition. The DP_{small} \rightarrow DP_{CD69+}/SP transition is not associated with proliferation (Mingueneau et al, 2013), facilitating the comparison of the $\alpha\beta$ TCR-induced signature with our $\gamma\delta$ TCR-induced signature which is pruned of genes involved in the cell cycle (Fig EV3B). It permitted to deconvolute the $\gamma\delta$ TCR-induced signature into a component expressed in the sole DN3b $\gamma\delta^+$ cells (denoted as the “ $\gamma\delta$ TCR only signature”) and a component expressed in both DN3b $\gamma\delta^+$ and DP_{CD69+}/SP cells (denoted as the “ $\gamma\delta$ and $\alpha\beta$ TCR shared signature”; Figs 4D–F and EV2D). The $\gamma\delta$ TCR-only signature comprised the *Etv5* and *Sox13* transcripts that code for transcription factors specifying the effector function of T $\gamma\delta$ 17 cells, *Blk*, a Src family PTK implicated in T $\gamma\delta$ 17-cell development (Laird et al, 2010), and *Cpa3* which codes for carboxypeptidase A3 (Turchinovich & Hayday, 2011). The $\gamma\delta$ and $\alpha\beta$ TCR shared signature comprised of *Klf2*; *Sesn3*, coding for a member of the sestrin family of stress-induced proteins; *Clec2d*, coding for a member of the natural killer cell receptor C-type lectin family; *Itgb2*, coding for an integrin β chain also known as LFA-1; *Tes*, coding for a scaffold protein playing a role in the actin cytoskeleton; *Cd53*, coding for a member

Figure 4. Transcriptional footprint of $\gamma\delta$ T-cell lineage commitment.

- A Dot plot showing the expression level of genes belonging to the $\gamma\delta$ TCR-induced signature across DN3a, DN3b $\gamma\delta^+$, DN4 $\gamma\delta^+$, DN3b $\gamma\delta^-$, and DN4 $\gamma\delta^-$ subsets of Dataset 1. The $\gamma\delta$ TCR-induced signature was defined by comparing the transcriptome of DN3b $\gamma\delta^-$ and DN3b $\gamma\delta^+$ cells (see Methods).
- B, C AUCell scores for the $\gamma\delta$ TCR-induced signature among the UMAP plot of cells corresponding to Dataset 1 (B) and Dataset 2 (C). As shown in Fig EV2, Dataset 2 corresponds to DN-enriched scRNAseq data merged with whole thymus scRNAseq data.
- D Dot plot showing the expression level of genes belonging to the $\gamma\delta$ TCR-induced signature across the cell subsets corresponding to Dataset 2. Based on the gene set that was specifically upregulated during the DP_{small} \rightarrow DP_{CD69+}/SP transition (see Fig EV3B), it allowed to subdivide the $\gamma\delta$ TCR-induced signature into a “ $\gamma\delta$ TCR only” signature and a “ $\alpha\beta$ and $\gamma\delta$ TCR shared” signature.
- E, F AUCell scores for the “ $\alpha\beta$ and $\gamma\delta$ TCR shared” signature (left panel) and for the “ $\gamma\delta$ TCR only” signature (right panel) among the UMAP plot of cells corresponding to Datasets 1 (E) and 2 (F).

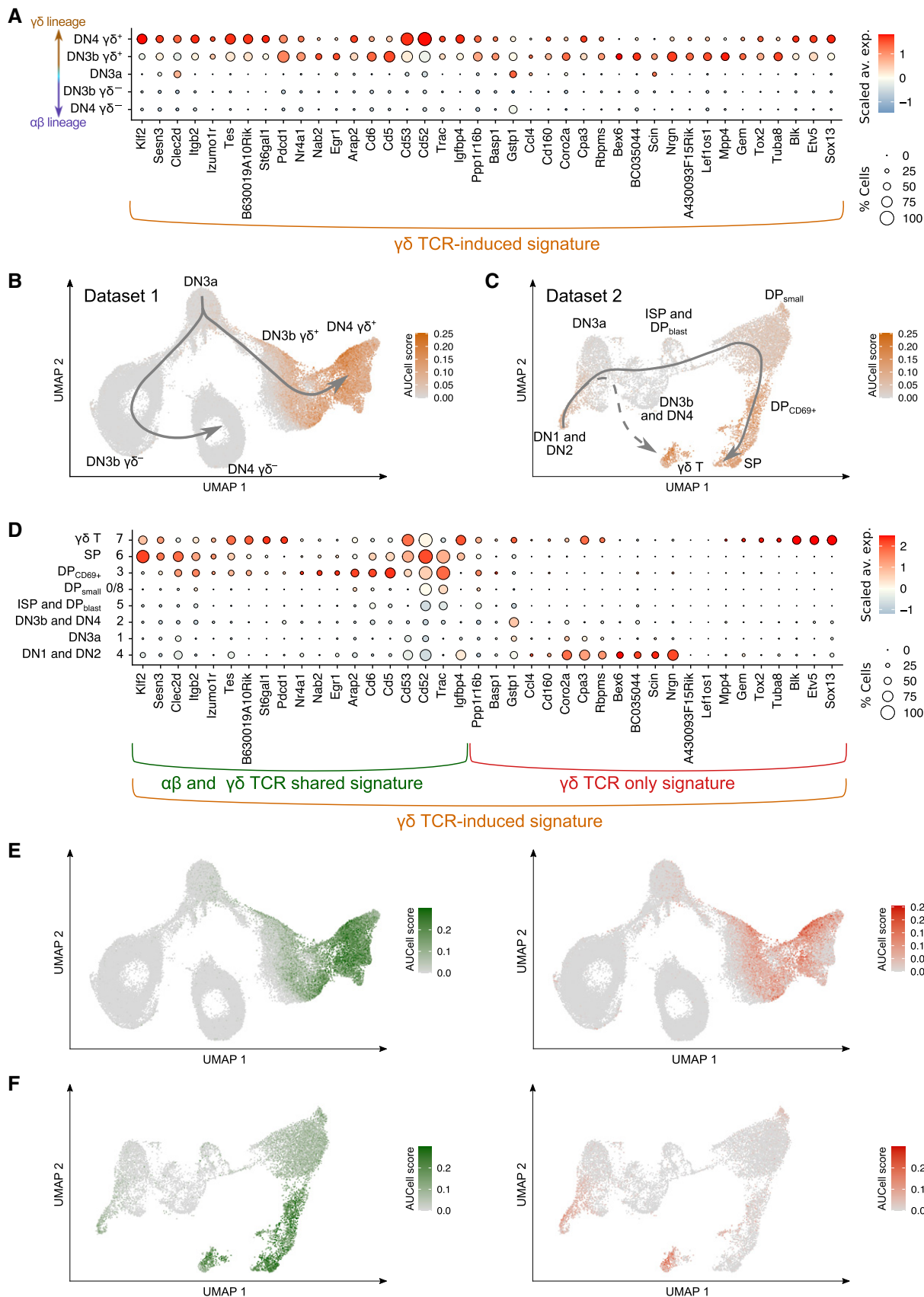


Figure 4.

of the transmembrane 4 superfamily; and *Cd52*, coding for CAMPATH-1, as well as transcripts coding for the CD5 and CD6 transmembrane receptors which both play an important role in regulating TCR signals (Mori *et al* (2021); Fig EV3B). Therefore, apart from the genes involved in the cell cycle and in metabolic activity, the transcriptional signature induced by the $\gamma\delta$ TCR at the DN3a \rightarrow DN3b $\gamma\delta^+$ transition was more similar to that induced by the $\alpha\beta$ TCR at the DP_{small} \rightarrow DP_{CD69+/SP} transition than to that induced by the pre-TCR.

scRNAseq analysis of adult DN3 cells expressing signaling-defective $\gamma\delta$ TCR

To support on the basis of genetic evidence the role of $\gamma\delta$ TCR-triggered signals in $\gamma\delta$ T-cell lineage commitment and specification, we exploited *Trdc-H2BEGFP* mice (Prinz *et al*, 2006). Those mice expressed an eGFP reporter gene under the control of the gene coding for the TCR δ chain, facilitating tracking of the earliest steps of $\gamma\delta$ T-cell lineage commitment. T-cell development is blocked at the DN3 stage in *Trdc-H2BEGFP* mice deficient for the LAT adaptor protein (*Lat*^{-/-} \times *Trdc-H2BEGFP* mice) (Nunez-Cruz *et al*, 2003), suggesting that LAT is required for both pre-TCR and $\gamma\delta$ TCR signaling. Approximately 0.3% of the DN3 cells found in *Lat*^{-/-} \times *Trdc-H2BEGFP* thymus expressed intermediate level of $\gamma\delta$ TCR at their surface (denoted in short as DN3 $\gamma\delta^{\text{int}}$ cells; Fig EV4A), demonstrating that progression beyond such DN3 $\gamma\delta^{\text{int}}$ stage is controlled by $\gamma\delta$ TCR signals requiring the LAT adaptor (Prinz *et al*, 2006). Moreover, the lack of CD5 expression and of CD127 downregulation on those LAT-deficient DN3 $\gamma\delta^{\text{int}}$ cells suggested that at least part of the $\gamma\delta$ T-cell specification program was not induced in the absence of instructive $\gamma\delta$ TCR signals (Prinz *et al*, 2006). Consistent with that view, infection of LAT-deficient DN3 $\gamma\delta^{\text{int}}$ cells with LAT-expressing retrovirus induced the surface expression of CD5 and of high levels of $\gamma\delta$ TCR as observed on a fraction of WT DN3b $\gamma\delta^+$ cells (Muro *et al*, 2019).

scRNAseq approaches offer the unprecedented possibility to analyze with single-cell resolution the transcriptome of those rare LAT-deficient DN3 $\gamma\delta^{\text{int}}$ cells. More specifically, it offered the opportunity to determine whether the expression of a $\gamma\delta$ TCR at their surface was associated with most hallmarks of $\gamma\delta$ T-cell lineage specification (Fig 4), or constituted their unique $\gamma\delta$ T-cell lineage marker. This last occurrence will formally demonstrate at single-cell resolution that the signals delivered by the $\gamma\delta$ TCR-LAT axis have an instructive role in adult $\gamma\delta$ T-cell lineage commitment. Using a workflow similar to that developed for WT DN thymocytes (Fig 1A), the LAT-deficient DN3 $\gamma\delta^-$ and LAT-deficient DN3 $\gamma\delta^{\text{int}}$ cell subsets found in *Lat*^{-/-} \times *Trdc-H2BEGFP* thymus were sorted and subjected to scRNAseq (Fig EV4B and C). After controlling the quality of our sequencing data (see Materials and Methods), the resulting

LAT-deficient DN3 $\gamma\delta^-$ and LAT-deficient DN3 $\gamma\delta^{\text{int}}$ cell datasets comprised of 7704 and 5979 cells, respectively, that were merged with Dataset 1 to generate Dataset 3. The UMAP plot corresponding to Dataset 3 had the same overall shape as that obtained for Dataset 1 (Figs 2 and 5A). A $\gamma\delta$ T-cell and $\alpha\beta$ T-cell lineage branches emerged from DN3a cells and LAT-deficient DN3 $\gamma\delta^-$, and LAT-deficient DN3 $\gamma\delta^{\text{int}}$ cells were located on the $\alpha\beta$ T-cell lineage branch in close contiguity to WT DN3a cells (Fig 5A).

Signaling-proficient $\gamma\delta$ TCR is required to commit DN3 $\gamma\delta^{\text{int}}$ cells to the $\gamma\delta$ T-cell lineage

To confirm that the positions occupied by the LAT-deficient DN3 $\gamma\delta^-$ and LAT-deficient DN3 $\gamma\delta^{\text{int}}$ cells within the UMAP were consistent with their transcriptomics profile, we used the Seurat FindAllMarkers function to define marker genes for each of the seven sorted samples of Dataset 3 and filtered them to keep only the top 25 DEG (see Materials and Methods). As expected on the basis of former work (Mingueneau *et al*, 2013), the top DEG of WT DN3a cells comprised transcripts coding for components of the Notch signaling pathway (*Notch3*) and for the Notch targets *Hes1*, *Il2ra*, and *Ptcra* (Fig 5B and C). Most of them were downregulated in WT thymus at the DN3a \rightarrow DN3b $\gamma\delta^-$ and DN3a \rightarrow DN3b $\gamma\delta^+$ transitions. WT DN3a cells shared 9 of the top 25 DEG with LAT-deficient DN3 $\gamma\delta^-$ and LAT-deficient DN3 $\gamma\delta^{\text{int}}$ cells. The top DEG common to WT DN3a, LAT-deficient DN3 $\gamma\delta^-$ and LAT-deficient DN3 $\gamma\delta^{\text{int}}$ stages corresponded to *Ptcra*, *Rag1*, and *Notch3* and were all repressed in WT DN3b $\gamma\delta^+$ cells.

The top DEG of both WT DN3b $\gamma\delta^+$ and WT DN3b $\gamma\delta^-$ cells corresponded to genes linked to the cell cycle and to high metabolic activity. As expected, they were downregulated in WT DN4 $\gamma\delta^+$ cells and remained expressed in WT DN4 $\gamma\delta^-$ cells. Consistent with our previous result (Fig EV1), the sole $\alpha\beta$ T-cell lineage mark identified among the WT DN4 $\gamma\delta^-$ top DEG corresponded to *Cd8b1*. In contrast, several genes among the top WT DN3b $\gamma\delta^+$ and DN4 $\gamma\delta^+$ DEG constituted hallmarks of the $\gamma\delta$ T-cell lineage (*Sox13*, *Maf*, and *Cpa3*), and those genes were absent or faintly expressed by LAT-deficient DN3 $\gamma\delta^{\text{int}}$ cells (Fig 5B and C). As a result, the LAT-deficient DN3 $\gamma\delta^{\text{int}}$ cells showed very low AUCell scores for the TCR $\gamma\delta$ -induced signature and its $\gamma\delta$ TCR only and $\gamma\delta$ and $\alpha\beta$ TCR shared components (Fig 6A–C). Importantly, LAT-deficient DN3 $\gamma\delta^{\text{int}}$ cells did not express *Cd8b1*, the sole hallmark of early $\alpha\beta$ T-cell specification (Fig 5B and C). Therefore, in the absence of a functional $\gamma\delta$ TCR-LAT signaling axis, no blatant mark of $\gamma\delta$ T-cell lineage specification can be found in DN3 $\gamma\delta^{\text{int}}$ cells aside from $\gamma\delta$ TCR expression. Signaling-proficient $\gamma\delta$ TCR is thus required to commit DN3 $\gamma\delta^{\text{int}}$ cells to the $\gamma\delta$ T-cell lineage, formally demonstrating that our $\gamma\delta$ TCR-induced signature is indeed fully induced by the $\gamma\delta$ TCR and does not contain components pre-existing to $\gamma\delta$ TCR induction.

Figure 5. Single-cell RNAseq analysis of DN3 $\gamma\delta^-$ and DN3 $\gamma\delta^{\text{int}}$ cells from *Lat*^{-/-} thymus.

- A, B UMAP plots of Dataset 3 which contains five WT (DN3a, DN3b $\gamma\delta^+$, DN4 $\gamma\delta^+$, DN3b $\gamma\delta^-$, and DN4 $\gamma\delta^-$) and two *Lat*^{-/-} (DN3 $\gamma\delta^-$ and DN3 $\gamma\delta^{\text{int}}$) scRNAseq datasets. The UMAP plot is colored according to sorted samples (A), and to expression levels of the specified genes (B).
- C Heatmap showing scaled expression of top 25 DEG characterizing each of the seven sorted samples of Dataset 3. The names of the sorted samples are specified at the top of the heatmap, and 3,000 cells were randomly selected for each sample. Each column represents the expression profile of a single cell. The sample from which a DEG is derived is indicated by colored bars on the left. Bar superpositions specify DEG that are found in more than one sample. The genes displayed in panel B are highlighted with a star. Gene expression is color coded with a scale based on z-score distribution, from -2 (purple) to 2 (yellow).

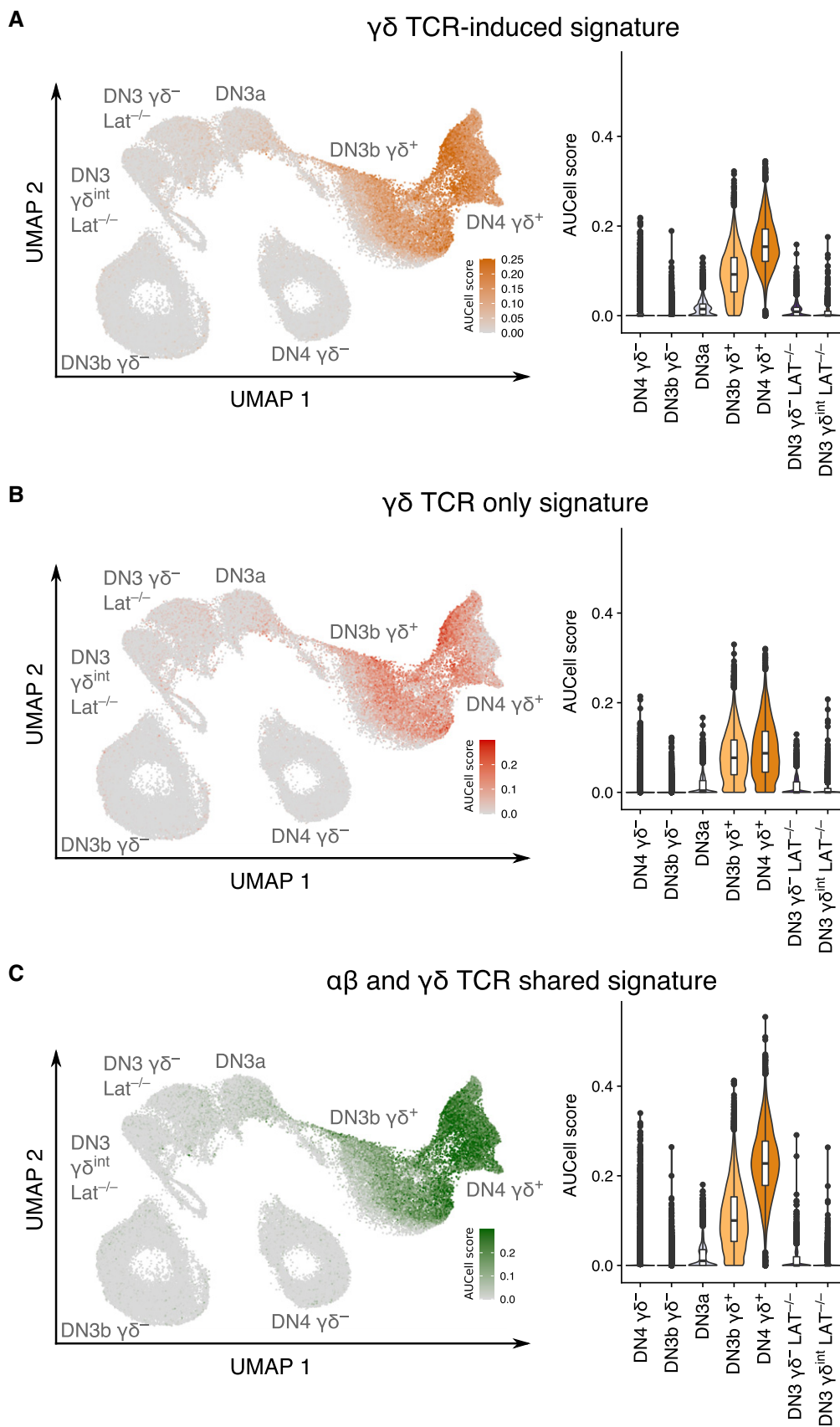


Figure 6.

Figure 6. *Lat*^{-/-} DN3 $\gamma\delta^{\text{int}}$ T cells do not express the $\gamma\delta$ lineage commitment signature.

A-C AUCell scores for the $\gamma\delta$ TCR-induced signature (A), $\gamma\delta$ TCR-only signature (B), and $\alpha\beta$ and $\gamma\delta$ TCR shared signature (C) are displayed on UMAP (left) and violin (right) plots of the seven sorted subsets corresponding to Dataset 3. As expected, AUCell scores for the three signatures were very low for DN3a cells, low for WT DN3b $\gamma\delta^-$ and WT DN4 $\gamma\delta^-$ cells, and high for WT DN3b $\gamma\delta^+$ and WT DN4 $\gamma\delta^+$ cells.

Revisiting the tightness of the developmental blockade occurring in *Lat*^{-/-} thymus

The lack of LAT is thought to induce a tight developmental blockade preventing DN3a cells to progress further along the $\alpha\beta$ and $\gamma\delta$ paths (Zhang *et al*, 1999; Nunez-Cruz *et al*, 2003; Muro *et al*, 2015). Unexpectedly, single-cell resolution analysis of the cycling status of the DN3 and DN4 subsets of Dataset 3 showed that approximately 25% of LAT-deficient DN3 $\gamma\delta^{\text{int}}$ cells were in S and G2M phases of the cell cycle as compared to 79% in WT DN3b $\gamma\delta^+$ (Fig 7A and B). It suggested that in the absence of LAT, the $\gamma\delta$ TCR expressed at the surface of DN3 $\gamma\delta^{\text{int}}$ cells was still capable of delivering LAT-independent signals to DN3 $\gamma\delta^{\text{int}}$ cells leading a quarter of them to embark into the cell cycle. By revisiting the flow cytometry data corresponding to the DN3 cells found in *Lat*^{-/-} thymus, we also found that approximately 30% of the LAT-deficient DN3 $\gamma\delta^{\text{int}}$ cells expressed CD71 (Appendix Fig S2), a hallmark of pre-TCR and $\gamma\delta$ TCR signaling (Fig 2D; Kelly *et al*, 2007). Moreover, minute numbers of LAT-deficient DN4 $\gamma\delta^{\text{int}}$ cells were also observed (Fig EV4A). Therefore, in contrast to former reports, the developmental blockade resulting from the lack of LAT is not as tight as previously described.

Our single-cell resolution analysis offered us the unique opportunity to determine at the transcriptional level whether the cycling LAT-deficient DN3 $\gamma\delta^{\text{int}}$ cells that likely received some LAT-independent $\gamma\delta$ TCR signals differed from the non-cycling LAT-deficient DN3 $\gamma\delta^{\text{int}}$ cells and showed some hints of $\gamma\delta$ T-cell specification. Accordingly, we reorganized the heatmap corresponding to the seven samples of Dataset 3 based on their cell cycling status (G0/G1, S, or G2/M; Fig 7C). It confirmed that most of the WT DN3b $\gamma\delta^-$ /DN4 $\gamma\delta^-$ cells and WT DN3b $\gamma\delta^+$ top DEG were characteristic of highly cycling cells (*Mki67*, *Ccnb1*, *Ccnb2*, *Nusap1*, *Rrm2*, *Cdca3*, *Birc5*, *Ube2c*, *Cenpm*, *Prc1*, *Cenpf*, *Ccna2*, *Hist1h1b*, *Hist1h4d*, *Hist1h2ae*, *Pfdn4*, *Fbxo5*, *Rmnd5a*, *Cenpw*, and *Ckk1*), and were switched off in the G0/G1 cells present in the seven analyzed cell subsets. The WT DN3a top DEG were repressed during the transition to WT DN3b $\gamma\delta^-$ and WT DN3b $\gamma\delta^+$ cells. The LAT-deficient DN3 $\gamma\delta^{\text{int}}$ cells that were in S and G2/M also repressed the WT DN3a DEG but to a smaller extent than WT DN3b $\gamma\delta^-$ and DN3b $\gamma\delta^+$ cells. Most remarkably, none of the WT DN3b $\gamma\delta^+$ and DN4 $\gamma\delta^+$ top DEG, which primarily corresponded to genes involved in $\gamma\delta$ T-cell differentiation and function, was induced in LAT-deficient DN3 $\gamma\delta^{\text{int}}$ cells, including those that managed to enter the

cell cycle. Therefore, even the LAT-deficient DN3 $\gamma\delta^{\text{int}}$ cells that started cycling via LAT-independent $\gamma\delta$ TCR signals were unable to turn on the program associated with $\gamma\delta$ T-cell lineage commitment. Accordingly, our data formally demonstrate at single-cell resolution that the $\gamma\delta$ TCR-LAT signaling axis exerts a key inductive role in adult $\gamma\delta$ T-cell lineage commitment and specification.

Discussion

We investigated at single-cell resolution the developmental bifurcation leading to $\alpha\beta$ and $\gamma\delta$ T-cell lineage specification in the thymus of adult WT mice and mice deprived of the LAT adaptor. It offered the unique possibility to compare the transcriptome of DN3a and $\gamma\delta$ -selected WT DN3b $\gamma\delta^+$ cells to that of DN3 cells that succeeded in expressing a $\gamma\delta$ TCR but failed delivering LAT-dependent signals. It demonstrated at single-cell resolution that $\gamma\delta$ TCR signals build upon a transcriptomic cell state that shows no sign of $\gamma\delta$ T-cell lineage commitment, and thus that signaling-proficient $\gamma\delta$ TCR is required to commit DN3 cells to the $\gamma\delta$ T-cell lineage. We also defined at single-cell level, the commonalities and differences in the transcriptional signatures resulting from pre-TCR, $\gamma\delta$ TCR, and $\alpha\beta$ TCR signaling at distinct stages of adult intrathymic development. Genes encoding several markers of signal strength (*Cd69*, *Cd5*, and *Nr4a1*) were induced by the pre-TCR, the $\gamma\delta$ TCR, and the $\alpha\beta$ TCR in DN3b $\gamma\delta^+$, DN3b $\gamma\delta^-$ /DN4 $\gamma\delta^-$, and DP cells, respectively. Consistent with the signal strength model of $\alpha\beta$ versus $\gamma\delta$ T-cell lineage commitment, the magnitude of their induction was lower during β selection as compared to $\gamma\delta$ selection, as well as to $\alpha\beta$ selection (Figs 4 and EV3). Moreover, the transcriptional signature induced by the $\gamma\delta$ TCR at the DN3a \rightarrow DN3b $\gamma\delta^+$ transition was more similar to that induced by the $\alpha\beta$ TCR at the DP_{small} \rightarrow DP_{CD69+}/SP transition than to the pre-TCR signature. Consistent with previous reports (Mingueneau *et al*, 2013; Taniuchi, 2018; Rothenberg, 2019), conventional DP_{CD69+}/SP cells differed, however, from DN4 $\gamma\delta^+$ cells in that they postponed most of their functional specialization after they leave the thymus and receive cytokine signals from antigen-laden dendritic cells in the periphery.

Both the DN3b $\gamma\delta^+$ cells and DN3b $\gamma\delta^-$ /DN4 $\gamma\delta^-$ cells constitute “transit-amplifying cells” that after dividing rapidly progress to differentiate into mature $\gamma\delta$ and $\alpha\beta$ T cells, respectively. To obtain the same fine-grained picture of these “transit-amplifying cells,” we

Figure 7. Impact of the cell cycle status on the scRNAseq expression profiles of DN3 $\gamma\delta^-$ and DN3 $\gamma\delta^{\text{int}}$ cells from *Lat*^{-/-} thymus.

A UMAP plots of sorted cell subsets from Dataset 3 colored according to cell cycle phases.
 B Bar plot showing the percentage of cells in the G0/G1 (red bars), S (blue bars), and G2/M (green bars) phases of the cell cycle among each of the seven sorted cell subsets of Dataset 3.
 C Heatmap showing scaled expression of up to 25 DEG from each of the seven sorted cell subsets of Dataset 3. In contrast to Fig 5C, the analyzed cells were further subdivided according to cell cycle phases (G0/G1, S, and G2/M) and 100 cells were randomly selected and analyzed per sample and per phase. The origin of each cell sample is indicated above columns and the color code corresponding to each seven sorted cell subsets is indicated at the bottom of the heatmap. A green star indicates that in the case of DN3a cells, only 32 cells were in G2/M phase and analyzed.

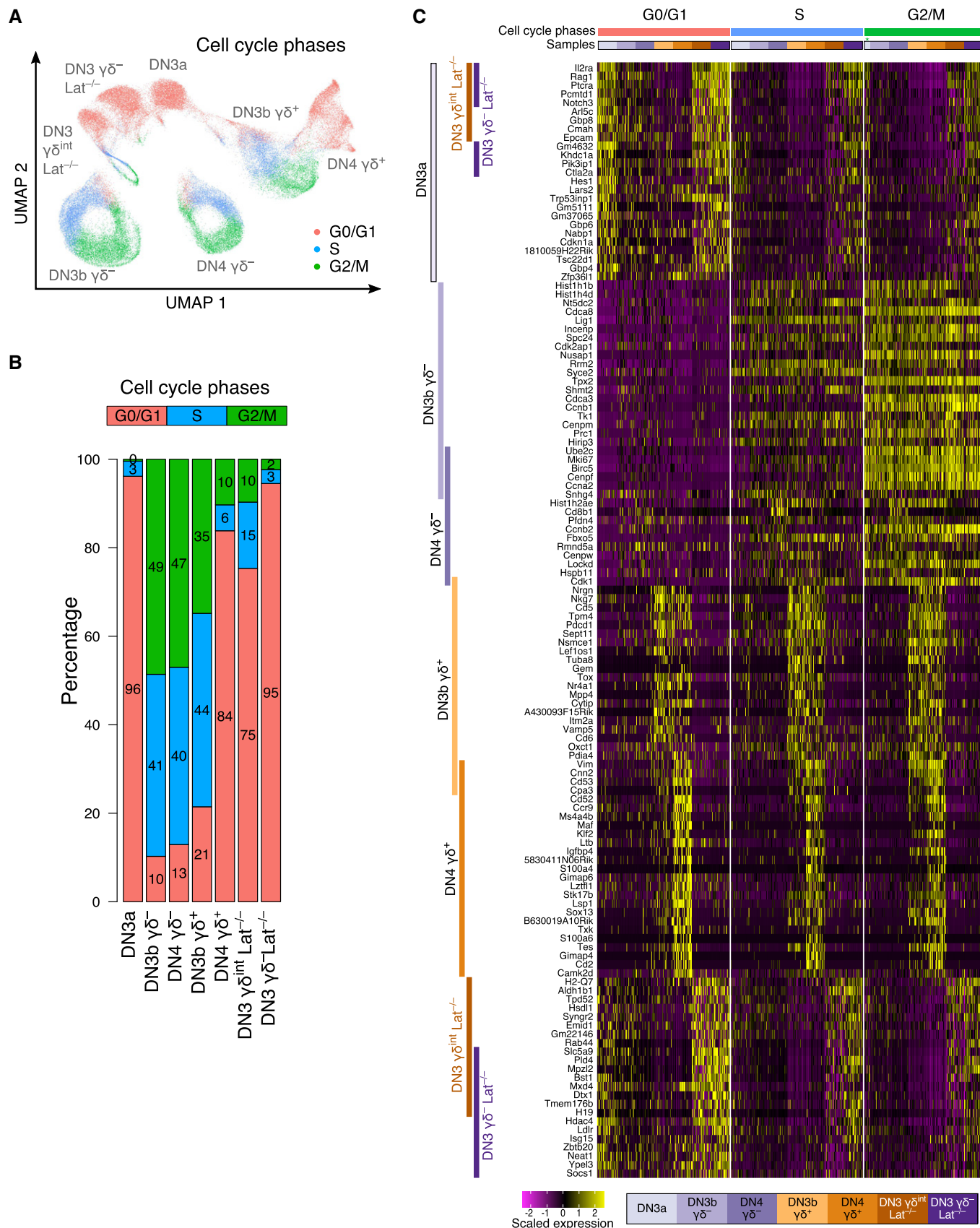


Figure 7.

subjected comparable numbers of sorted DN3b $\gamma\delta^+$, DN3b $\gamma\delta^-$, and DN4 $\gamma\delta^-$ cells to scRNAseq. However, it is important to emphasize that the DN3b $\gamma\delta^+$ and DN3b $\gamma\delta^-$ /DN4 $\gamma\delta^-$ cells correspond to 0.4% and 25%, respectively, of adult DN cells. Therefore, the presence in an adult thymus of approximately 300-fold more DP cells (the direct progeny of DN4 $\gamma\delta^-$ cells) than DN4 $\gamma\delta^+$ cells (the direct progeny of DN3b $\gamma\delta^+$ cells) is commensurate to the sizes of the DN3b $\gamma\delta^+$ and DN3b $\gamma\delta^-$ /DN4 $\gamma\delta^-$ “transit-amplifying cell” compartments. These distinct sizes might result from the distinct mitogenic capacity of the pre-TCR and $\gamma\delta$ TCR, and/or from the lower occurrence among DN3a cells of coincident productive *Trg* and *Trd* gene rearrangements as compared to that of productive *Trb* gene rearrangements.

Our single-cell resolution analysis also demonstrated that the heterogeneity present among DN3b $\gamma\delta^+$, DN3b $\gamma\delta^-$, and DN4 $\gamma\delta^-$ cells was primarily due to their distinct cycling status, whereas that found in DN4 $\gamma\delta^+$ cells reflected their diversification into distinct $\gamma\delta$ T-cell effector subsets. In contrast, DN3a cells were more homogeneous, suggesting that after assembling in DN3a cells, the pre-TCR and $\gamma\delta$ TCR use the same signal transduction machinery. Therefore, the different developmental outcomes resulting from the firing of the pre-TCR and $\gamma\delta$ TCR have to result from their distinct subunit architectures or ligand dependence (Dutta *et al*, 2021). In addition, the pre-TCR and $\gamma\delta$ TCR do not work in isolation and other receptors contribute to enforce $\alpha\beta$ and $\gamma\delta$ T-cell lineage specification (Dutta *et al*, 2021). Likewise, the effector programming of DN4 $\gamma\delta^+$ cells subsets also depends on environmental cues, such as cytokines, and costimulatory molecules (Fiala *et al*, 2020; Chen *et al*, 2021).

In mature $\alpha\beta$ T cells, TCR-triggered signals divide into multiple branches at the level of the plasma membrane, resulting in the formation of multiple signalosomes nucleating around transmembrane receptors or adaptors such as LAT, CD6, CD5, and LAX1 (Mori *et al*, 2021). They contribute to TCR signal diversification and to the initiation of negative feedback loops. Accordingly, in the absence of LAT, TCR engagement in mature $\alpha\beta$ T cells still induce a partial signaling cascade that prevents the differentiation of effector T cells (Mingueneau *et al*, 2009). Akin to LAT-deficient mature $\alpha\beta$ T cells, cross-linkage of the $\gamma\delta$ TCR expressed on LAT-deficient DN3 $\gamma\delta^{\text{int}}$ cells failed to induce ERK phosphorylation but triggered normal levels of AKT phosphorylation (Muro *et al*, 2018). Therefore, the partial LAT-independent $\gamma\delta$ TCR signals induced in LAT-deficient DN3 $\gamma\delta^{\text{int}}$ cells likely account for the entry into the cell cycle of 0.3% of them and in turn to their aborted progression beyond the DN4 stage. Although our study provides an unprecedented single-cell resolution picture of the role of $\gamma\delta$ TCR signaling in the specification of the adult $\gamma\delta$ -T cell lineage, one of its limitations must be noted. It results from the extremely low surface expression of the pre-TCR on DN3 cells as compared to that of the $\gamma\delta$ TCR, a feature precluding identification of pre-TCR⁺ DN3 cells in WT and LAT-deficient mice and in turn the definition of their single-cell transcriptome.

In conclusion, our study demonstrated that $\gamma\delta$ TCR signals build upon a $\gamma\delta$ T-cell uncommitted transcriptomic state to initiate $\gamma\delta$ T-cell lineage specification in DN3 cells of adult thymus, a result supporting the instructive model of $\gamma\delta$ T-cell lineage commitment. In addition, the single-cell resolution afforded by scRNAseq

provided a more complete view of the first checkpoint encountered by developing T cells and of the extent of its perturbation in the absence of the LAT adaptor. Charting the distinct signal transduction networks at the basis of successful β selection and $\gamma\delta$ selection remains an important challenge owing to the small numbers of early developing T cells in which those events occur. Most single-cell studies focus on nucleic acids and, as long as specific antibodies are available, on proteins and post-translational modifications. However, protein complexes, rather than individual protein, are the functional units of signaling pathways, suggesting that new advances in single-cell proteomics and interactomics by mass spectrometry will help further comparison of the β -selection and $\gamma\delta$ -selection checkpoints.

Materials and Methods

Mice

Mice were bred under specific pathogen-free conditions in CIPHE animal facilities and handled in accordance with Institutional Committee and European guidelines for animal care. C57BL/6 mice were purchased from Janvier Labs and *Lat*^{-/-} x *Trdc-H2BEGFP* mice have been described (Prinz *et al*, 2006).

Cell preparation

Cells from thymus and spleen were extracted as described in the IMPRESS protocol (<https://www.mousephenotype.org/impress/ProcedureInfo?procID=201>). Briefly, organs were disrupted using OctoGentleMACS system (Miltenyi Biotec) with 35 mg collagenase II (Serlabo) and 50 μ g DNase I (Sigma) for 20 min at room temperature (RT). Enzymatic reaction was stopped with EDTA (10mM, Invitrogen). Red blood cells present in spleens were lysed for 1 min at RT using an ammonium-chloride-potassium (ACK) lysis solution (eBioscience). Cell suspensions were filtered with 70 μ m cell strainers (BD Falcon) and counted using Sytox Green or Sytox Red (Invitrogen) to exclude dead cells.

Depletion of CD4⁺, CD8⁺, and CD4⁺CD8⁺ cells from thymus

Cells extracted from pooled thymus were depleted of CD4⁺, CD8⁺, and CD4⁺CD8⁺ T cells using Dynabeads Mouse CD4 and Dynabeads Mouse CD8 according to the manufacturer’s protocol (Invitrogen Life Technologies). Proper depletion was validated by staining the resulting cell suspension with anti-CD4-BV421 (RM4-5), anti-CD8 α -PE (53-7.3), and anti-CD8 β -PE (H35-17.2) antibodies from BD Biosciences. The remaining DN-enriched thymocytes were stained with dead cell marker Sytox Green (Invitrogen) and then live cells were counted on an Attune NXT system (Life Technologies).

Flow cytometry analysis

Samples were first stained with Fixable Viability Stain 440 UV (BD Biosciences), and incubated for 15 min on ice with anti-CD16/32 antibody (clone 2.4G2) to block Fc receptors. Samples were then stained with the following antibodies CD3 ϵ -BB700 (145-2C11),

CD4-BUV737 (RM4-5), CD8 α -BV650 (53-6.7), CD25-BUV395 (PC61), CD27-PE (LG.3A10), CD69-BV605 (H1.2F3), CD117-PE-CF594 (2B8), and CD161-APC-Cy7 (PK136), all from BD Biosciences, with CD5-PE-Cy7 (53-7.3), CD24-A700 (M1/69), CD44-APC (IM7), and CD71-BV421 (RI7217), all from Biolegend, and with TCR δ -PE-Cy5 (GL-3) from Invitrogen. Multiparameter FACS acquisition was performed on a Fortessa LSRII SORP system (BD Biosciences) and data analyzed with FACSDiva 9.0 (BD Biosciences) and FlowJo 10.7.1 (BD Biosciences) software. Doublets were systematically excluded based on side scatter (SSC) and forward scatter (FSC) parameters.

Antibodies

Antibodies used for flow cytometry are listed in Appendix Table S1.

Preparation of single-cell RNA-sequencing libraries

DN3-DN4 cell libraries generation

Total *Lat*^{-/-} *x Trdc-H2BEGFP* thymocytes and DN-enriched WT thymocytes were labeled with CD3 ϵ -BB700 (145-2C11), CD4-BUV737, CD8 α -APC (53-6.7), CD25-BUV395, CD44-PE, CD69-BV605, CD117-PE-CF594, and CD161-BV650, all from BD Biosciences; CD5-PE-Cy7, CD24-A700, and CD71-BV421, all from Biolegend; and TCR δ -PE-Cy5 (Invitrogen). For both types of samples, DAPI (Invitrogen) was used as a viability dye. DN thymocyte subsets were sorted as specified in Figs 1A and EV4B using a BD FACSAria SORP (BD Biosciences). Doublets were systematically excluded based on side scatter (SSC) and forward scatter (FSC) parameters. Mouse splenic B cells (CD19⁺MHC class II⁺) were sorted after labeling with CD19 (1D3) and IA-IE (M5/114.15.2) both from BD Biosciences, and were used as internal standard for generating Datasets 1 and 3. After sorting, cells were washed in PBS (Sigma-Aldrich), supplemented with 0.04% BSA (Sigma-Aldrich), and counted using Attune NXT system (Thermo Fischer Scientific). A total of 18,000 sorted cells corresponding to each of the five DN thymocyte subsets of interest were spiked with 500 sorted splenic B cells, and then loaded on a Chromium Chip B (one cell-subset per well), and droplet encapsulated with a Chromium Controller (10X Genomics). Single-cell cDNA synthesis and sequencing libraries were prepared with Chromium Single Cell 3' v3 Library and Gel Bead kit (10X Genomics) according to manufacturer's instructions.

DN-enriched and total WT thymocyte libraries generation

DN-enriched and total WT thymocyte suspensions were sorted based on viability using DAPI (Invitrogen) as specified in Fig EV2A using a BD FACSAria SORP (BD Biosciences). Doublets were systematically excluded based on SSC and FSC parameters. Thawed human PBMC (huPBMC) cells were counted using Sytox Green (Invitrogen), stained with DAPI (Invitrogen), sorted for live cells, and were used as an internal standard for generation of Dataset 2. After sorting, cells were washed and counted as described above. A total of 18,000 sorted cells corresponding either to live DN thymocytes or to live total thymocytes were spiked with 5,000 sorted live huPBMC, then loaded on a Chromium Chip B (one cell-subset per well) and droplet-encapsulated with a Chromium Controller (10X Genomics). Single-cell cDNA synthesis and sequencing libraries were prepared as described above.

Sequencing and data analysis

Sequencing was performed by Macrogen (Seoul, South Korea) on an Illumina HiSeq X platform and the following parameters were applied: Read 1:26 cycles; i7:8 cycles; and Read 2:57 cycles. mRNA libraries were preprocessed using Cell Ranger count (version 5.0.1).

Generation of datasets 1 and 3

Dataset 1

Sequencing reads obtained from DN3-DN4 subsets sorted from WT and *Lat*^{-/-} *x Trdc-H2BEGFP* thymus were aligned to a modified version of the mm10 mouse genome containing the *Trdc-H2BEGFP* edited version of the *Trdc* gene and quantified. The mRNA data matrices were imported into R (v3.6.3) and downstream analysis was performed with the Seurat package (version 3.1.5) (Butler *et al*, 2018; Stuart *et al*, 2019). Low-quality cells corresponding to cells expressing < 200 genes or > 15% of mitochondrial-associated genes were filtered out and genes expressed in less than three cells were removed. The five WT sorted samples (DN3a, DN3b $\gamma\delta^-$, DN4 $\gamma\delta^-$, DN3b $\gamma\delta^+$, and DN4 $\gamma\delta^+$) were first merged with the Seurat merge function. Before mRNA expression analysis, *Trdc-H2BEGFP* and *Trdc* gene counts were summed up in a single feature called "Trdc." Then, expression raw counts were normalized and scaled using, respectively, the Seurat NormalizeData and ScaleData functions. The top 2,000 variable genes were selected (FindVariableFeatures function; selection method = "vst") to perform a dimensionality reduction using the principal component analysis method (RunPCA function), and a UMAP was computed using the 20 first components (RunUMAP function). Cell clusters were identified using Seurat FindClusters function with Louvain Algorithm option (using 20 dimensions and a resolution of 1). We filtered out unwanted cell clusters (non-T cells, B-cell/T-cell doublets, and low-quality cells having a low percentage of ribosomal genes). Then, to obtain Dataset 1, we reselected the most 2,000 variable genes and performed a second UMAP dimensionality reduction (with RunPCA and RunUMAP functions using 30 dimensions and k.param option 50) and clustering with a resolution of 0.4. To analyze $\gamma\delta$ lineage diversification, we selected cells corresponding DN3a to DN4 $\gamma\delta^+$ T cells and switched to a finer clustering resolution (1.5).

Dataset 3

To generate Dataset 3, we added the *Lat*^{-/-} *x Trdc-H2BEGFP* sorted samples (*Lat*^{-/-} DN3 $\gamma\delta^-$ and *Lat*^{-/-} DN3 $\gamma\delta^{\text{int}}$) to the five sorted WT samples (DN3a, DN3b $\gamma\delta^-$, DN4 $\gamma\delta^-$, DN3b $\gamma\delta^+$, and DN4 $\gamma\delta^+$) using the Seurat merge function and proceeded as described previously for Dataset 1. Considering that the spike-in B cells from the *Lat*^{-/-} DN3 $\gamma\delta^{\text{int}}$ were not properly superimposed because of a different proportion of ribosomal mRNA, we regressed out the proportion of ribosomal mRNA using the Seurat scaledata function. To obtain a UMAP plot where B cells were properly superimposed, we recalculated the UMAP coordinates and clustering (30 dimensions and resolution 1). To obtain Dataset 3, we filtered out unwanted clusters and reselected the 2,000 most variable genes to perform UMAP dimensionality reduction (using 50 dimensions and k.param option 50) and clustering with a resolution of 0.4 corresponding to a merged and cleaned Dataset 3.

Generation of dataset 2

Using CellRanger, sequencing reads from whole WT thymus and from WT DN-enriched samples were aligned to the GRCh38/mm10 mouse and human composite genome and gene count were quantified. Gene expression matrix was slimmed down to keep only mm10 features using CollapseSpeciesExpressionMatrix function and human/mouse cell doublets were removed. Low-quality cells were also filtered out (i.e., cells expressing < 200 genes or > 10% of mitochondrial-associated genes) and genes expressed in less than three cells were removed. Expression raw counts were then normalized using Seurat NormalizeData function and samples were merged with Seurat merge function. The top 2,000 variable genes were selected (FindVariableFeatures function; selection method = “vst”) to perform a dimensionality reduction using the principal component analysis method (RunPCA function). A UMAP was computed using the 20 first components (RunUMAP function) and cells were clustered with the FindNeighbors (20 dimensions) and FindClusters (0.6 resolution) functions. Non-T-cell clusters were filtered out and the cell cycle variation effects were regressed out using the ScaleData function. To obtain a merged and cleaned Dataset 2, the top 2,000 variable genes were reselected to perform a second UMAP dimensionality reduction (using 30 dimensions) and clustering with a resolution of 0.42.

Gene expression analysis and statistical analysis

DEG were identified using the FindAllMarkers Seurat function with the default parameters (Wilcoxon rank sum test for genes with a minimum 0.25 log fold change between the two groups of cells and expressed in at least 10% of cells in either of the two populations tested). DEG between two samples were identified using the FindMarkers function using the same parameters as the FindAllMarkers Seurat function. For the $\gamma\delta$ TCR-induced signature, pre-TCR-induced signature, and top DEG markers of Dataset 3, we added a filter to keep only genes having an adjusted *P*-value of 0 and expressed in < 25% of the cells of the compared samples group (pct.2 < 25%). A *P*-value of 0 corresponds to *P*-value < $2.225074e^{-308}$ due to R limitations. Cell cycle phases were scored using the CellCycleScoring Seurat function. To identify cell samples in which a given signature is active, we assigned a signature score to each cell sample using AUCell.

Data availability

The transcriptomics data have been deposited in the Gene Expression Omnibus public database under accession number GSE184545 (<http://www.ncbi.nlm.nih.gov/geo/query/acc.cgi?acc=GSE184545>). GSE184545 comprises of two sub-series denoted as GSE184483 (<http://www.ncbi.nlm.nih.gov/geo/query/acc.cgi?acc=GSE184483>) and GSE184544 (<http://www.ncbi.nlm.nih.gov/geo/query/acc.cgi?acc=GSE184544>) corresponding to Datasets 1 and 3 and to Dataset 2, respectively.

Expanded View for this article is available online.

Acknowledgements

This work was supported by CNRS, INSERM, the MSDAvenir Fund (to B.M.), PHENOMIN (French National Infrastructure for Mouse Phenogenomics; ANR-

10-INBS-07, to B.M.), and the European Union's Horizon 2020 research and innovation program (grant agreement no 787300 (BASILIC) to B.M.), ITMO Cancer of AVIESAN (Alliance Nationale pour les Sciences de la Vie et de la Santé, National Alliance for Life Sciences & Health) within the framework of the Cancer Plan (project no C19046S to D.P.B.) and from CNRS “Osez l'interdisciplinarité!” program “DMATH” project (to D.P.B.), and by fellowships from the MSDAvenir Fund (S.S.), Fondation ARC (S.S.), and PHENOMIN (R.O.). We acknowledge Pierre Milpied and Laurine Gil for their advice on scRNAseq assays and Lionel Spinelli for his advices on bioinformatics analysis. Centre de Calcul Intensif d'Aix-Marseille Université is acknowledged for granting access to its high-performance computing resources.

Author contributions

Bernard Malissen: Conceptualization; Resources; Formal analysis; Supervision; Funding acquisition; Validation; Investigation; Methodology; Writing—original draft; Project administration; Writing—review & editing. **Sara Scaramuzzino:** Formal analysis; Validation; Investigation; Visualization; Methodology. **Delphine Potier:** Conceptualization; Data curation; Software; Formal analysis; Supervision; Validation; Investigation; Visualization; Methodology. **Robin Ordioni:** Investigation; Methodology. **Pierre Grenot:** Investigation; Methodology. **Dominique Payet-Bornet:** Data curation; Software; Formal analysis; Supervision; Validation; Investigation; Visualization; Methodology; Writing—original draft. **Hervé Luche:** Conceptualization; Supervision; Validation; Investigation; Methodology.

In addition to the CRediT author contributions listed above, the contributions in detail are:

BM and HL conceived the project, SS, PG, and RO generated the data, SS, DP-B, and DP analyzed the data and prepared the figures, and BM wrote the manuscript with contributions from all authors.

Disclosure and competing interests statement

The authors declare that they have no conflict of interest.

References

- Aibar S, González-Blas CB, Moerman T, Huynh-Thu VA, Imrichova H, Hulselmans G, Rambow F, Marine J-C, Geurts P, Aerts J *et al* (2017) SCENIC: single-cell regulatory network inference and clustering. *Nat Methods* 14: 1083–1086
- Butler A, Hoffman P, Smibert P, Papalexi E, Satija R (2018) Integrating single-cell transcriptomic data across different conditions, technologies, and species. *Nat Biotechnol* 36: 411–420
- Carlson CM, Endrizzi BT, Wu J, Ding X, Weinreich MA, Walsh ER, Wani MA, Lingrel JB, Hogquist KA, Jameson SC (2006) Kruppel-like factor 2 regulates thymocyte and T-cell migration. *Nature* 442: 299–302
- Chen ELY, Lee CR, Thompson PK, Wiest DL, Anderson MK, Zuniga-Pflucker JC (2021) Ontogenic timing, T cell receptor signal strength, and Notch signaling direct gammadelta T cell functional differentiation *in vivo*. *Cell Rep* 35: 109227
- Ciofani M, Knowles GC, Wiest DL, von Boehmer H, Zuniga-Pflucker JC (2006) Stage-specific and differential notch dependency at the alphabeta and gammadelta T lineage bifurcation. *Immunity* 25: 105–116
- Contreras AV, Wiest DL (2020) Recent advances in understanding the development and function of gammadelta T cells. *F1000Research* 9: 306–316
- Dong G, Zhang S, Shen S, Sun L, Wang X, Wang H, Wu J, Liu T, Wang C, Wang H *et al* (2020) SPATS2, negatively regulated by miR-145-5p,

- promotes hepatocellular carcinoma progression through regulating cell cycle. *Cell Death Dis* 11: 837
- Dutta A, Zhao B, Love PE (2021) New insights into TCR beta-selection. *Trends Immunol* 42: 735–750
- Fiala GJ, Gomes AQ, Silva-Santos B (2020) From thymus to periphery: molecular basis of effector gammadelta-T cell differentiation. *Immunol Rev* 298: 47–60
- Haks MC, Lefebvre JM, Lauritsen JP, Carleton M, Rhodes M, Miyazaki T, Kappes DJ, Wiest DL (2005) Attenuation of gammadeltaTCR signaling efficiently diverts thymocytes to the alphabeta lineage. *Immunity* 22: 595–606
- Hayday AC (2019) gammadelta T cell update: adaptate orchestrators of immune surveillance. *J Immunol* 203: 311–320
- Hayes SM, Li L, Love PE (2005) TCR signal strength influences alphabeta/gammadelta lineage fate. *Immunity* 22: 583–593
- Hosokawa H, Rothenberg EV (2021) How transcription factors drive choice of the T cell fate. *Nat Rev Immunol* 21: 162–176
- Ivanov II, McKenzie BS, Zhou L, Tadokoro CE, Lepelley A, Lafaille JJ, Cua DJ, Littman DR (2006) The orphan nuclear receptor ROR γ directs the differentiation program of proinflammatory IL-17+ T helper cells. *Cell* 126: 1121–1133
- Kelly AP, Finlay DK, Hinton HJ, Clarke RG, Fiorini E, Radtke F, Cantrell DA (2007) Notch-induced T cell development requires phosphoinositide-dependent kinase 1. *EMBO J* 26: 3441–3450
- Klein F, Mitrovic M, Roux J, Engdahl C, von Muenchow L, Alberti-Servera L, Fehling HJ, Pelczar P, Rolink A, Tsapogas P (2019) The transcription factor Duxbl mediates elimination of pre-T cells that fail beta-selection. *J Exp Med* 216: 638–655
- Kreslavsky T, Savage AK, Hobbs R, Gounari F, Bronson R, Pereira P, Pandolfi PP, Bendelac A, von Boehmer H (2009) TCR-inducible PLZF transcription factor required for innate phenotype of a subset of gammadelta T cells with restricted TCR diversity. *Proc Natl Acad Sci U S A* 106: 12453–12458
- Laird RM, Laky K, Hayes SM (2010) Unexpected role for the B cell-specific Src family kinase B lymphoid kinase in the development of IL-17-producing gammadelta T cells. *J Immunol* 185: 6518–6527
- Livak F, Tourigny M, Schatz DG, Petrie HT (1999) Characterization of TCR gene rearrangements during adult murine T cell development. *J Immunol* 162: 2575–2580
- Malissen B, Ardouin L, Lin SY, Gillet A, Malissen M (1999) Function of the CD3 subunits of the pre-TCR and TCR complexes during T cell development. *Adv Immunol* 72: 103–148
- Melichar HJ, Narayan K, Der SD, Hiraoka Y, Gardiol N, Jeannot G, Held W, Chambers CA, Kang J (2007) Regulation of gammadelta versus alphabeta T lymphocyte differentiation by the transcription factor SOX13. *Science* 315: 230–233
- Mingueneau M, Kreslavsky T, Gray D, Heng T, Cruse R, Ericson J, Bendall S, Spitzer MH, Nolan GP, Kobayashi K et al (2013) The transcriptional landscape of alphabeta T cell differentiation. *Nat Immunol* 14: 619–632
- Mingueneau M, Roncagalli R, Grégoire C, Kissenpfennig A, Miazek A, Archambaud C, Wang Y, Perrin P, Bertosio E, Sansoni A et al (2009) Loss of the LAT adaptor converts antigen-responsive T cells into pathogenic effectors that function independently of the T cell receptor. *Immunity* 31: 197–208
- Mori D, Grégoire C, Voisinne G, Celis-Gutierrez J, Aussel R, Girard L, Camus M, Marcellin M, Argenty J, Burlet-Schiltz O et al (2021) The T cell CD6 receptor operates a multitask signalosome with opposite functions in T cell activation. *J Exp Med* 218
- Munoz-Ruiz M, Ribot JC, Grosso AR, Goncalves-Sousa N, Pamplona A, Pennington DJ, Regueiro JR, Fernandez-Malave E, Silva-Santos B (2016) TCR signal strength controls thymic differentiation of discrete proinflammatory gammadelta T cell subsets. *Nat Immunol* 17: 721–727
- Muro R, Nitta T, Okada T, Ideta H, Tsubata T, Suzuki H (2015) The Ras GTPase-activating protein Rasal3 supports survival of naive T cells. *PLoS One* 10: e0119898
- Muro R, Nitta T, Nakano K, Okamura T, Takayanagi H, Suzuki H (2018) gammadeltaTCR recruits the Syk/PI3K axis to drive proinflammatory differentiation program. *J Clin Invest* 128: 415–426
- Muro R, Takayanagi H, Nitta T (2019) T cell receptor signaling for gammadeltaT cell development. *Inflamm Regen* 39: 6
- Nunez-Cruz S, Aguado E, Richelme S, Chetaille B, Mura AM, Richelme M, Pouyet L, Jouvin-Marche E, Xerri L, Malissen B et al (2003) LAT regulates gammadelta T cell homeostasis and differentiation. *Nat Immunol* 4: 999–1008
- Oh S, Gray DHD, Chong MMW (2021) Single-cell RNA sequencing approaches for tracing T cell development. *J Immunol* 207: 363–370
- Palacios EH, Weiss A (2007) Distinct roles for Syk and ZAP-70 during early thymocyte development. *J Exp Med* 204: 1703–1715
- Parker ME, Ciofani M (2020) Regulation of gammadelta T cell effector diversification in the thymus. *Front Immunol* 11: 42
- Prinz I, Sansoni A, Kissenpfennig A, Ardouin L, Malissen M, Malissen B (2006) Visualization of the earliest steps of gammadelta T cell development in the adult thymus. *Nat Immunol* 7: 995–1003
- Prinz I, Silva-Santos B, Pennington DJ (2013) Functional development of gammadelta T cells. *Eur J Immunol* 43: 1988–1994
- Qu J, Bishop JM (2012) Nucleostemin maintains self-renewal of embryonic stem cells and promotes reprogramming of somatic cells to pluripotency. *J Cell Biol* 197: 731–745
- Roels J, Kuchmiy A, De Decker M, Strubbe S, Lavaert M, Liang KL, Leclercq G, Vandekerckhove B, Van Nieuwerburgh F, Van Vlierbergh P et al (2020) Distinct and temporary-restricted epigenetic mechanisms regulate human alphabeta and gammadelta T cell development. *Nat Immunol* 21: 1280–1292
- Rothenberg EV (2019) Programming for T-lymphocyte fates: modularity and mechanisms. *Genes Dev* 33: 1117–1135
- Rothenberg EV (2021) Single-cell insights into the hematopoietic generation of T-lymphocyte precursors in mouse and human. *Exp Hematol* 95: 1–12
- Sagar PM, Herman JS, Naik S, Sock E, Zeis P, Lausch U, Wegner M, Tanriver Y, Littman DR, Grun D (2020) Deciphering the regulatory landscape of fetal and adult gammadelta T-cell development at single-cell resolution. *EMBO J* 39: e104159
- Spidale NA, Sylvia K, Narayan K, Miu B, Frascoli M, Melichar HJ, Zhihao W, Kisielow J, Palin A, Serwold T et al (2018) Interleukin-17-producing gammadelta T cells originate from SOX13(+) Progenitors that Are Independent of gammadeltaTCR Signaling. *Immunity* 49: 857–872.e5
- Stuart T, Butler A, Hoffman P, Hafemeister C, Papalexi E, Mauck 3rd WM, Hao Y, Stoeckius M, Smibert P, Satija R (2019) Comprehensive integration of single-cell data. *Cell* 177: 1888–1902.e21
- Taghon T, Yui MA, Pant R, Diamond RA, Rothenberg EV (2006) Developmental and molecular characterization of emerging beta- and gammadelta-selected pre-T cells in the adult mouse thymus. *Immunity* 24: 53–64
- Taniuchi I (2018) CD4 helper and CD8 cytotoxic T cell differentiation. *Annu Rev Immunol* 36: 579–601
- Turchinovich G, Hayday AC (2011) Skint-1 identifies a common molecular mechanism for the development of interferon-gamma-secreting versus interleukin-17-secreting gammadelta T cells. *Immunity* 35: 59–68

Uehara S, Grinberg A, Farber JM, Love PE (2002) A role for CCR9 in T lymphocyte development and migration. *J Immunol* 168: 2811–2819

Zhang W, Sommers CL, Burshtyn DN, Stebbins CC, Dejarnette JB, Triple RP, Grinberg A, Tsay HC, Jacobs HM, Kessler CM *et al* (1999) Essential role of LAT in T cell development. *Immunity* 10: 323–332

Zhao B, Yoganathan K, Li L, Lee JY, Zuniga-Pflucker JC, Love PE (2019) Notch and the pre-TCR coordinate thymocyte proliferation by induction of the SCF subunits Fbxl1 and Fbxl12. *Nat Immunol* 20: 1381–1392

Zuberbuehler MK, Parker ME, Wheaton JD, Espinosa JR, Salzler HR, Park E, Ciofani M (2019) The transcription factor c-Maf is essential for the commitment of IL-17-producing gammadelta T cells. *Nat Immunol* 20: 73–85



License: This is an open access article under the terms of the Creative Commons Attribution License, which permits use, distribution and reproduction in any medium, provided the original work is properly cited.